c.3

STRANGE PARTICLE PRODUCTION IN π^+p INTERACTIONS NEAR 3.7 GeV/c

RECEIVED
LAWRENCE
RADIATION LABORATORY

AUG 11 1970

LIBRARY AND
DOCUMENTS SECTION

William Ralph Butler
(Ph.D. Thesis)

May 29, 1970

AEC Contract No. W-7405-eng-48

TWO-WEEK LOAN COPY

This is a Library Circulating Copy which may be borrowed for two weeks. For a personal retention copy, call Tech. Info. Division, Ext. 5545

UCRL-19845

LAWRENCE RADIATION LABORATORY
UNIVERSITY of CALIFORNIA BERKELEY

c.2

DISCLAIMER

This document was prepared as an account of work sponsored by the United States Government. While this document is believed to contain correct information, neither the United States Government nor any agency thereof, nor the Regents of the University of California, nor any of their employees, makes any warranty, express or implied, or assumes any legal responsibility for the accuracy, completeness, or usefulness of any information, apparatus, product, or process disclosed, or represents that its use would not infringe privately owned rights. Reference herein to any specific commercial product, process, or service by its trade name, trademark, manufacturer, or otherwise, does not necessarily constitute or imply its endorsement, recommendation, or favoring by the United States Government or any agency thereof, or the Regents of the University of California. The views and opinions of authors expressed herein do not necessarily state or reflect those of the United States Government or any agency thereof or the Regents of the University of California.

STRANGE PARTICLE PRODUCTION IN π^+p INTERACTIONS NEAR 3.7 GeV/c

Contents

Abstract v

I. Introduction 1

II. Scanning and Measuring 2

III. Cross Sections 6

A. Proton Contamination 6

B. Normalization 7

C. Strange Particle Scanning Efficiency 9

D. Decays 10

1. Decays of Charged Hyperons 11

2. Vees 12

E. Λ vs Σ^o 13

F. Other Ambiguities 15

G. Summary 17

IV. Resonance Production 21

A. $\Sigma^+K^*(890)^+$ and $\Sigma(1385)^+K^+$ 22

B. $pK^+\overline{K^o}$ 25

C. $p\pi^+K\overline{K}$ 26

1. $p\pi^+K^+K^-$ 28

2. $p\pi^+K^o\overline{K^o}$ 31

V. Some Physical Characteristics of the Data 33

A. Σ^+K^+ t Distribution 34

B. $\Sigma(1385)^+K^+$ t and Decay Distributions 35

C. $\pi^+p \rightarrow \Delta^{++}\varphi$ and SU_3 36

D. Suppression of Other States in $p\pi^+K\bar{K}$ 37

VI. Summation 39

Acknowledgments 40

Appendix 41

References 47

Figure Captions 49

STRANGE PARTICLE PRODUCTION IN π^+p INTERACTIONS NEAR 3.7 GeV/c

William Ralph Butler*

Lawrence Radiation Laboratory
University of California
Berkeley, California

May 29, 1970

ABSTRACT

We present cross sections for both stable and resonant strange particle final states produced by the interactions of positive pions in hydrogen. The data are taken from several incident momenta between 3.56 GeV/c and 3.82 GeV/c. We find the overall strange particle cross section to be about 1.5 mb. We present two favorable tests of line reversal by comparing $\pi^+p \rightarrow Y^+K^+$ with $K^-p \rightarrow Y^+\pi^-$, where Y^+ first represents Σ^+ and then $\Sigma(1385)^+$. In a detailed study of the final state $p\pi^+K\bar{K}$, we find: (a) $\sigma(\pi^+p \rightarrow p\pi^+\varphi) = 10\pm3$ μb, but $\sigma(\pi^+p \rightarrow \Delta^{++}\varphi) \leq 2$ μb; (b) both the Δ^{++} and the $K^*(890)$ are prominent structures in this four-body final state; (c) the $K\bar{K}$ state occurring with the Δ^{++} is either K_1K_1 or K^+K^- in even parity angular momentum states; however no threshold enhancement is associated with the Δ^{++}.

---

*On leave from David Lipscomb College, Nashville, Tennessee.

Table I. Reactions of primary interest.

i.	$\pi^+ p \rightarrow \Sigma^+ K^+$
ii.	$\rightarrow \Sigma^+ \pi^+ K^o$
iii.	$\rightarrow \Sigma^+ \pi^o K^+$
iv.	$\rightarrow \Lambda \pi^+ K^+$
v.	$\rightarrow \Sigma^o \pi^+ K^+$
vi.	$\rightarrow p K^+ \bar{K}^o$
vii.	$\rightarrow p \pi^+ K^+ K^-$
viii.	$\rightarrow p \pi^+ K^o \bar{K}^o$
ix.	$\rightarrow \Lambda \pi^+ \pi^o K^+$
x.	$\rightarrow \Lambda \pi^+ \pi^+ K^o$
xi.	$\rightarrow \Sigma^o \pi^+ \pi^+ K^o$
xii.	$\rightarrow \Sigma^+ \pi^+ \pi^o K^o$
xiii.	$\rightarrow \Sigma^+ \pi^+ \pi^- K^+$
xiv.	$\rightarrow \Sigma^- \pi^+ \pi^+ K^+$

II. SCANNING AND MEASURING

Approximately forty percent of the film was scanned for all interactions within a given scanning fiducial volume. In the remainder of the film, ordinary two-prong events without stopping protons were omitted. In the context of this study, "ordinary" will describe an event with no strange particle signature, such as a kink in a charged track, or a vee associated with the event. Note that interaction vii of Table I occurs primarily as an ordinary event. We refer to any interaction topology having at least one kink or vee as a "strange particle event." Each

topology is assigned an event type number corresponding to the number of prongs, kinks, and vees it possesses. (See Fig. 1.)

The first measurement of the events was performed on the Flying Spot Digitizer (FSD). Geometric reconstruction and kinematic analysis was done through the program SIOUX (combined TVGP[2] and SQUAW[3]).

To obtain the beam momentum profile for each section of film, we fit the ordinary four-prong events for the following four-constraint hypotheses:

$$\pi^+ p \rightarrow p\pi^+\pi^+\pi^- \qquad (1)$$

$$\pi^+ p \rightarrow p\pi^+ K^+ K^- \qquad (2)$$

$$pp \rightarrow pp\pi^+\pi^- \quad . \qquad (3)$$

From the sample of events which fit reaction (1) unambiguously, we histogram the fitted momentum of the beam track. Then we fit a Gaussian function to this distribution to obtain an average value and a raw root mean square (rms) width. From the distribution of the calculated errors in the fitted momentum of the beam track, we determine the mean error, or resolution, of the fitting procedure to be about ±0.025 GeV/c. This mean error is then subtracted in quadrature from the raw rms width to give the final rms width.

The average value and rms width of the beam momentum are then used as input to the fitting procedure through the technique known as "beam-averaging." For each event, the measured beam track momentum and the mean value described above are averaged with weights inversely proportional to their respective errors. This "beam-averaged" momentum is then used for the measured momentum of the beam track in the kinematic analysis.

For the strange particle events, the output from the SIOUX program was compared to each event at the scan table in order to make visual identification of tracks by ionization (track bubble density) and to correct mistakes made by the initial scanner. Interactions having only pi decays and/or electron pairs were removed from the strange particle category. Except for about thirty percent which were remeasured on the FSD, failing strange particle events were remeasured on on-line Franckenstein measuring projectors. The above process was repeated and a second measurement was performed on the Franckensteins for those events which failed again.

The remeasurement of ordinary events has not been completed at the time of this writing. However, for about 30% of the film, the ordinary events have been processed in the same manner described in the preceding paragraph. For the remainder of the film, only the first measurement of the ordinary events is available. This situation has bearing on reaction vii of Table I and on the normalization for cross sections.

An accepted strange particle event hypothesis must satisfy the following criteria:

1. The coordinates (x, y, z) of the interaction vertex must satisfy

$$-14 \leq x \leq +12 \text{ cm},$$

$$-63 \leq y \leq +50 \text{ cm, and}$$

$$+14 \leq z \leq +20 \text{ cm}.$$

   The coordinate system is defined in Fig. 2.

2. The beam track momentum must lie within three standard deviations of the mean value momentum for that region. Similarly the azimuthal (φ) and dip (λ) angles for the beam track must lie within

three standard deviations of the window defined by

$$85.6^{\circ} \leq \varphi \leq 91.2^{\circ}, \text{ and}$$

$$-1.8^{\circ} \leq \lambda \leq 2.0^{\circ}.$$

Before applying the criteria, the values of the momentum, azimuth, and dip are extrapolated to $y = 0$ to correct for energy loss and the curvature due to the magnetic field.

3. The geometric reconstruction is adequate in the sense that the point scatter on each track is consistent with the setting error plus multiple scattering, and that the tracks come together at the vertex within the errors.
4. The hypothesis is consistent with the track bubble densities as seen on the scan table.
5. If the hypothesis is a constrained fit, then the confidence level is greater than 0.01. If the hypothesis is not constrained at the primary vertex, then the missing mass is consistent with two or more missing neutrals and the missing momentum is greater than zero.

When more than one hypothesis are acceptable, we accept only the highest constraint hypothesis. The one exception to this rule is the case of Λ vs Σ^{0} hypothesis which will be discussed in the next section. If more than one hypothesis of the same constraint class are acceptable, all are recorded and the event is tagged as ambiguous.

The scanning efficiency for all events is determined by a second scan of eight rolls. The rescan events are subjected to the same acceptance criteria as the first scan. After correction for very low momentum transfer elastic scatters, the single scan efficiency for finding an

event is 98%. The statistical error on this number is so small that systematic effects dominate the uncertainty. Table II gives the results of the rescan for all events. The scanning efficiencies pertinent to the strange particle topologies are discussed in the next section.

Table II. Results of single scan efficiency determination.

	Accepted events found on this scan but not on the other		Accepted events found on both scans	Total
	Non-elastic	Elastic		
First scan	84	100	4177	4361
Second scan	70	59	4177	4306

III. CROSS SECTIONS

A. Proton Contamination

Protons represent a significant source of contamination in this experiment, especially at the highest momentum, 4.0 GeV/c. For this reason, we omit all rolls containing film taken at this highest momentum. In the remainder of the film, those events which fit uniquely the reaction $pp \rightarrow pp\pi^+\pi^-$ were taken as a measure of the proton contamination. The effects of the protons are subtracted out using the information from two rolls of pure proton film and scaling according to the number of unique $pp\pi^+\pi^-$ fits in the pion film. To reduce still further these effects, we also remove rolls where the ratio of $pp \rightarrow pp\pi^+\pi^-$ fits to all unique 4 prong - 4 constraint fits exceeds 20%. This removal deletes 20 rolls; omitting the highest momentum deletes 31 rolls. The total deletion amounts to about 20% of the film.

Fortunately, the strange particle production due to proton-proton interactions is small in the momentum region of our experiment.[4] Therefore the major effect of the proton correction on the pion strange particle cross sections is in the normalization through the subtraction described in the preceding paragraph.

B. Normalization

In principle, we want to normalize the total number of accepted events to the known total cross section for π^+p interactions as determined by precision counter experiments. However there are difficulties in implementing this procedure in addition to the proton contamination just discussed. As was mentioned in Section II, only in 40% of the film were all topologies recorded; furthermore, only 30% of the ordinary events have been processed to the same extent as the strange particle events. In view of this situation, we adopt the following procedure:

(a) We use the number of 4-prong events scanned as a secondary standard for the normalization. Actually, we want the number of 4-prong events due to incident pions. Therefore for any section of film we consider, we subtract the number of 4-prongs scanned due to protons as determined from the proton rolls and scaled as described above.

(b) In the 30% of the film where all events have been processed, we obtain the ratio of the total number of accepted events to the total number of 4-prong events scanned. Again we want the number of accepted events due to pions; thus we subtract the number of accepted events due to protons as determined from the proton rolls and scaled as described above.

(c) In the remainder of the film, the (expected) number of accepted events is given by the ratio from step (b) multiplied by the number of 4-prongs scanned in that part of the film.

The above procedure allows us to calculate the total number of acceptable events for the section of film we use. Then this number is normalized to the total cross section for π^+p interactions at this momentum. Because our statistics are limited we do not intend to separate the momentum regions, and therefore our cross sections will be averages for the momentum interval spanned by the experiment, 3.71 ± 0.15 GeV/c.

The π^+p total cross section has been measured very precisely for this momentum region.[5] The value ranges from 28.2 mb at our lowest momentum, 3.56 GeV/c to 28.0 mb at 3.82 GeV/c, which is the highest momentum used in this study. At the momentum represented by our largest block of film, the cross section is very near 28.1 mb, which is also the value obtained from a weighted average over the momenta present in this study. Therefore we take as our standard cross section, the value 28.1 mb. Table III shows the microbarn equivalents for various sections of film considered in this experiment. The actual details of the calculation are presented in the Appendix. It should be noted that the scanning efficiency is not included in the numbers.

Table III. Microbarn equivalents for different sections.

Total sample	(0.234±0.004) μb/event
All events processed	(0.712±0.011) μb/event
All events recorded	(0.553±0.009) μb/event
Not all events recorded*	(0.407±0.007) μb/event

*Omits 2-prongs without stopping protons.

C. Strange Particle Scanning Efficiency

Losses of strange particle events due to scanning inefficiency are of two types. The first is a missed event; the second is an event which is found but is not recognized as a strange particle event type. The final state $p\pi^+K^+K^-$ does not suffer from the second loss. Such an event with a decay becomes an ordinary 4-prong if the decay is not recognized; the $p\pi^+K^+K^-$ hypothesis is tried whether or not the decay is measured.

In view of the high scanning efficiency for all events as discussed in Section II, the first category does not appreciably affect the strange particle events. In order to determine the scanning efficiency for strange particles, we conduct a special scan over ten rolls. Each roll is scanned by two different scanners looking only for strange particle event types. These two scans are combined with the original scan to give the total sample of strange particle events in the ten rolls. As before, these events are subjected to the same acceptance criteria as the original scan. This total sample is compared against the original scan to measure the efficiency. New events on the rescan were measured and processed in the same manner as the first scan. The total number of accepted strange particle events on these ten rolls is 367.

Separate efficiencies are calculated for these categories of events: (a) events with at least one vee, (b) events with only charged decays, one of which is the type hyperon goes to charged pion plus neutral baryon, (c) events with only charged decays, one of which is $\Sigma^+ \rightarrow p\pi^o$. These efficiencies are calculated separately for the section of film where all events were recorded and for the section of film where some two-prongs were omitted. Table IV shows these efficiencies. In view of the low efficiency for hyperon to charged pion decays in the second section of film, we will use only the first section for cross-section calculations.

Table IV. Strange particle single scan efficiencies.

Category	Vee events	Charged pion decays of hyperons	$\Sigma^+ \rightarrow p\pi^o$
All events recorded	0.98±0.01	0.89±0.04	0.73±0.07
Not all events recorded*	0.90±0.03	0.64±0.10	0.50±0.09

*Omits 2-prongs without stopping protons.

D. Decays

In this analysis we consider the following decays:

<u>positive decays</u> $\Sigma^+ \rightarrow p\pi^o$ (4)

$\Sigma^+ \rightarrow n\pi^+$ (5)

<u>negative decays</u> $\Sigma^- \rightarrow n\pi^-$ (6)

$\Xi^- \rightarrow \Lambda\pi^-$ (7)

neutral decays $K^o \rightarrow \pi^+\pi^-$ (8)

$\Lambda \rightarrow p\pi^-$ (9)

In most cases, charged K decays were also measured. However, due to the long $K^{\pm}$ lifetime, these decays represent only about 10% of all K's produced. Therefore, any final state which is detected by charged K decays alone is very biased (against fast $K^{\pm}$) and will not be discussed here.

1. Decays of Charged Hyperons

For the purpose of determining cross sections for Σ^+ production only the decay (5) is used. The decay (4) is eliminated because the angle between the Σ^+ and the outgoing proton is small, resulting in considerably lower scanning efficiency than for (5). In the discussion that follows, we use decay (5) as an example; however the comments apply equally well to decays (6) and (7).

The loss of events from (5) are due to three reasons. First, a sigma may decay so close to the production vertex that the decay is not visible. Second, the laboratory angle between the Σ^+ and the outgoing π^+ may be so small that they appear to be one track. Third, the plane of the decay may be nearly parallel to the camera axis, in which case the projected decay angle in each view is small and the two tracks again appear as one. The loss due to charged decays outside the decay fiducial volume (see next section) is negligible since the baryons are mostly peripheral and have shorter lifetimes than the lambda hyperon (for which the loss is small, but not negligible).

To remedy the first effect, we weight each event by the factor $\exp(+\tau_m/\tau)$, where τ_m is the proper time required to go the minimum distance required of a decay and τ is the proper lifetime of the particle. The minimum distance required is 5 mm. Kinematics does not allow a Σ^+ to be produced with a momentum less than about 330 MeV/c. This momentum corresponds to a range of about 12 cm in liquid hydrogen; thus there is no value of momentum for which the Σ^+ is never seen. Similar statements can be made for Σ^- and Ξ^-.

To deal with the other two effects, we look at a sample of events with the decay (5). For these events, Figure 3 shows a scatter plot of the decay cosine in the sigma center of mass versus the azimuth of the decay about the direction of the sigma. Normally the range of the azimuth is 0° to 360°, but here it is shown folded twice so that 0° means only that the plane of the decay is perpendicular to the z-axis and 90° means that the plane of the decay contains the z-axis. Although this plot should have uniform density, there is a definite depletion of events for forward decays and for decays with azimuths near 90°. To correct for this depletion, we eliminate events which are in the region from 0.7 to 1.0 in decay cosine, or the region 80° to 90° in azimuth. The remaining events are weighted by the ratio of the total area of the plot to the area of the plot after the cuts.

2. <u>"Vees"</u>

The following decay fiducial volume is applied to neutral decays (vees):

$$-17 \leq x \leq 20 \text{ cm},$$

$$-65 \leq y \leq 70 \text{ cm, and}$$

$$6 \leq z \leq 30 \text{ cm} .$$

Neutral decays outside these limits are ignored. Also the same minimum length is required of the neutral track as is required of charged decays. We therefore weight each vee event by the factor $(e^{-\tau_m/\tau} - e^{-\tau_f/\tau})^{-1}$. The quantities τ_m and τ are the same here as for charged decays. The quantity τ_f is the proper time required for the vee to reach the edge of the decay fiducial volume. A scatter plot of decay cosine vs decay azimuth does not reveal any appreciable loss of neutral decays due to small angle decays.

E. Λ vs Σ^0

At the beginning of this experiment, it was not clear that accepting the highest constraint class hypothesis would properly separate, event by event, the two hypotheses

$$\pi^+ p \rightarrow \Lambda \pi^+ K^+ \tag{10}$$

$$\text{and} \quad \pi^+ p \rightarrow \Sigma^0 \pi^+ K^+ \tag{11}$$

We therefore accepted both fits if both passed the criteria set forth above, even though (11) is a lower constraint class than (10). The same procedure was followed for reactions x and xi of Table I.

For each of the set of events ambiguous between hypotheses (10) and (11), we transform the entire event to the Σ^0 rest frame. For this set of ambiguous events, we then examine the distribution of the decay cosine of the photon from the Σ^0 decay with respect to each of the three measured tracks at the primary vertex--the beam, the outgoing pion and the kaon.

These distributions (Figs. 4a,b,c) have extremely sharp peaks in the forward direction, whereas each should be uniform for pure Σ^0 decay. Figure 4d shows a scatter plot of the decay cosine with respect to the outgoing pion versus the decay cosine with respect to the kaon, where events in the forward peak of the beam distribution (Fig. 4a) have been excluded. Almost all the events lie near the forward boundaries. We conclude therefore that all these events belong to hypothesis (10). Figure 4e shows the distribution of the decay cosine with respect to the beam for those events which fit (11) unambiguously. There is no appreciable loss of events in the forward direction indicating that the separation of the two hypotheses is complete. The cross section for reaction (11) is determined from the events which fit it unambiguously; all of the ambiguous events are assigned to reaction (10). The analogous assignment is made for the reactions x and xi of Table I.

The sharp peaks in Figs. 4a-c are qualitatively explained as follows (we discuss the beam as an example; similar arguments apply to the outgoing tracks): In order for reaction (10) to simulate reaction (11), the sigma-lambda mass difference of about 80 MeV must be manufactured by the kinematic fitting process. Since the longitudinal (along the beam) momentum balance is less well determined than the transverse momentum balance, the fitting will increase the beam momentum to give the necessary momentum to the photon without changing the other momenta too much. The relationship is easily visualized in the lambda rest frame where the photon momentum can absorb the entire change in beam momentum without changing the other momenta and at the same time approximately give the correct sigma mass. Since the lambda is peripheral,

the beam is still relativistic and changing the momentum gives an equal change in energy, which makes the beam behave like the photon. This analogy is more nearly valid if the photon is forward than if it is backward; in either case, the energy of the final state is increased by the presence of the photon, whereas for the backward photon, the energy of the initial state is decreased. Of course this solution does not give the minimum chi-square so that the other momenta are readjusted somewhat. We look at the decay distribution in the sigma rest frame because it should be uniform there for real sigmas; however this frame is practically the same as the lambda rest frame and the sharpness of the peak remains.

F. Other Ambiguities

The problem of events which fit more than one hypothesis of the same constraint class as present in reactions iii, viii, and ix of Table I. The remaining reactions are either unambiguous or have at least one topology in which no ambiguities occur. We deal with these ambiguities in the following manner: The number of events, N, assigned to one hypothesis is given by an equation of the form,

$$N = U + fA \tag{12}$$

where U is the number of unambiguous events for that hypothesis, A is the number of events ambiguous with that hypothesis, and f is the fraction of the ambiguous events that should actually contribute to that hypothesis. The fraction f may be obtained from a distribution, as in the Λ vs Σ^0 case, or from a topology in which no ambiguities occur, as for reaction (3) of Table I. In case f cannot be determined experimentally,

it is assigned the value 1/2 for double ambiguities, 1/3 for triple ambiguities and 1/4 for quadruple ambiguities. Then the error assigned to f is ± 0.25 in all three values.

When reaction iii of Table I is ambiguous, it is always ambiguous with reaction ii for which the K^o decays into neutral pions. Therefore we can determine how many events we expect for reaction ii from those events where the K^o decays into charged pions. This determination is, in effect, a determination of the fraction f in Eq. (12).

Reaction viii of Table I represents a unique situation. We have a topology where both vees are seen and a topology where only one vee is seen. When only one vee is seen, the event is often ambiguous with other hypotheses. (See Table VI.) The $K^o\overline{K^o}$ system may appear either as $K_1^oK_1^o$ or $K_2^oK_2^o$, or as $K_1^oK_2^o$ depending on the quantum numbers of its production. For the $K_1^oK_1^o$ system, we should see both decays about 47% of the time, only one decay about 43% of the time and neither decay 10% of the time. For the $K_1^oK_2^o$ system we should see the K_1 decay about 68% of the time. The point is, that in order to determine the cross section for $p\pi^+K_1^oK_2^o$, we must use the topology where only one vee is seen. Although we can determine how many $K_1^oK_1^o$ events are in this topology, there is no necessary relationship between that number and the number of $K_1^oK_2^o$ events. Therefore, for the topology in which only one vee is seen, we resort to the assignment for f described above.

In principle, reaction ix of Table I has a topology in which no ambiguities occur, namely, that one in which the K^+ decays. However, for the reasons discussed in part D of this section, we will not use this topology to determine f and there make the assignment for f described above.

G. Summary

The following tables summarize the input data and the results for the stable particle cross sections. Table V gives the values used for branching fractions, which were taken from the Particle Data Tables.[6] Table VI summarizes the event totals for various categories as well as the results of weighting with the decay factors discussed above. Table VII presents, for each channel considered, the final weighted numbers of events and the resulting cross sections corrected to include all decay modes.

Table V. Branching fractions taken from Ref. 6.

Decay	Branching fractions
$K_1^o \rightarrow \pi^+\pi^-$	0.684±0.011
$\Lambda \rightarrow p\pi^-$	0.653±0.012
$\Sigma^+ \rightarrow n\pi^+$	0.472±0.015

We use the fact that the $p\pi^+K_1^oK_1^o$ cross section is equal to the $p\pi^+K_2^oK_2^o$ in order to determine the total $p\pi^+K^o\overline{K^o}$ cross section. The total $p\pi^+K^o\overline{K^o}$ cross section is computed by adding twice the $p\pi^+K_1^oK_1^o$ to the $p\pi^+K_1^oK_2^o$ cross section.

We recall the following constraints discussed above. For any topology containing a vee, we use all of the restricted film sample. For a topology containing only a charged decay, we use only the section of film where all events are scanned. For the $p\pi^+K^+K^-$ final state, we use only the 30% of the film that has been fully processed for ordinary events.

Table VI. Data for cross-section determination.

Final state[a]	All events recorded: # hypotheses 1	2	3	4	Weighted total	Not all events recorded*: # hypotheses 1	2	3	4	Weighted total
Σ^+K^+	63	0	0	0	86±13	-	not used		-	-
$\Sigma^+\pi^+K^o_c$	20	0	0	0	24±7	28	0	0	0	44±9
$\Sigma^+\pi^+K^o_n$	34	40	0	0	160±16	-	not used		-	-
$\Sigma^+\pi^oK^+$	53	40	0	0		-	not used		-	-
$\Lambda_c\pi^+K^+$	101	0	0	0	108±11	138	0	0	0	147±13
$\Sigma^o\pi^+K^+$	49	0	0	0	50±7	60	0	0	0	64±8
$pK^+\overline{K^o_c}$	42	0	0	0	45±7	50	0	0	0	53±8
$p\pi^+K^+K^-$ [b]	112	0	0	0	112±11	-	not used		-	-
$p\pi^+K^o_cK^o_c$	16	0	0	0	16±5	23	0	0	0	26±6
$p\pi^+K^o_cK^o_n$	37	8	0	0	40±7	51	11	1	2	63±9
$\Lambda_c\pi^+\pi^oK^+$	106	43	0	0	137±17	144	57	0	0	186±21
$\Lambda_c\pi^+\pi^+K^o_c$	21	0	0	0	24±5	32	0	0	0	33±7
$\Sigma^o\pi^+\pi^+K^o_c$	7	0	0	0	8±3	11	0	0	0	13±4
$\Sigma^+\pi^+\pi^oK^o_c$	10	0	0	0	14±5	21	0	0	0	29±7
$\Sigma^+\pi^+\pi^-K^+$	64	0	0	0	91±12	-	not used		-	-
$\Sigma^-\pi^+\pi^+K^+$	28	0	0	0	32±7	-	not used		-	-

*Omits two-prongs without stopping protons.

(a) Subscript c means vee decay was observed. Subscript n means vee decay was not observed. We include only those Σ^+ events for which $\Sigma^+ \rightarrow n\pi^+$. We include only those Σ^o events for which $\Sigma^o \rightarrow \Lambda_c\gamma$.

(b) For this final state, we use only the 30% of the film for which all events are processed.

Table VII. Results of cross-section determinations.

Final state	Final weighted number[a]	Cross section[b] (μb)
Σ^+K^+	95±15	111±18
$\Sigma^+\pi^+K^o$	72±12	104±18
$\Sigma^+\pi^oK^+$	115±23	135±28
$\Lambda\pi^+K^+$	267±19	96±7
$\Sigma^o\pi^+K^+$	119±12	43±4
$pK^+\overline{K^o}$	103±11	70±8
$p\pi^+K^+K^-$	112±11	80±8
$p\pi^+K_1^oK_1^o$	44±8	22±4
$p\pi^+K_1^oK_2^o$	58±15	20±5
$p\pi^+K^o\overline{K^o}$	188±19	64±7
$\Lambda\pi^+\pi^oK^+$	338±29	121±11
$\Lambda\pi^+\pi^+K^o$	59±9	62±9
$\Sigma^o\pi^+\pi^+K^o$	22±5	23±6
$\Sigma^+\pi^+\pi^oK^o$	45±9	66±14
$\Sigma^+\pi^+\pi^-K^+$	100±14	118±17
$\Sigma^-\pi^+\pi^+K^+$	35±8	19±4

(a) Includes all scanning efficiency corrections, but does not include branching fraction corrections.

(b) Includes branching fraction corrections.

The errors quoted for the results are basically statistical. There may still be systematic effects present. In particular, it is quite likely that the final state $\Lambda\pi^+\pi^oK^+$ contains also events from the final state $\Sigma^o\pi^+\pi^oK^+$, which is not a constrained fit.

If we add together all our final states (including final states not listed in Table I) except those which have a charged K decay as their only signature, we find the cross section for this subset to be about 1.33 mb. From the charged K decays observed, our guess is that the final states having only charged K's (including reaction vii of Table I) will add about another 0.2 mb. Combining these two numbers gives 1.5 mb for the total strange particle cross section. As a point of interest, we mention the observance of a few events with Ξ final states, notably $\Xi^oK^+K^+$ and $\Xi^-\pi^+K^+K^+$; they correspond to a cross section of the order of a couple of microbarns.

It is interesting to make some comparison of our results with other experiments. A π^+p experiment[7] at 8 GeV/c has looked only at strange particle final states which contain vees. In addition, they fail to quote any Σ^o final states so that there are few states in common with the ones we examine. However from those few, we can say that the cross sections for three-body final states are falling off with incident momentum, whereas the cross section for the four-body final states seem to be about the same.

Table VIII shows a comparison of our results with a π^-p experiment[8] at 3.9 GeV/c. With one exception, the comparison consists of choosing final states where a positive pion in our experiment becomes a negative pion in the π^-p experiment. There are both remarkable similarities and differences.

Table VIII. $\pi^{\pm}p$ comparison of strange particle production.

Final state	Cross sections in μb	
	π^-p at 3.9 GeV/c[8]	π^+p at 3.7 GeV/c
$\Sigma^+K^o\pi^{\pm}$	42±8	104±18
$\Lambda K^+\pi^{\pm}$	99±13	96±7
$\Sigma^oK^+\pi^{\pm}$	43±7	43±4
$pK^+K^-\pi^{\pm}$	63±20	80±8
$pK_1^oK_1^o\pi^{\pm}$	12±4	22±4
$pK_1^oK_2^o\pi^{\pm}$	32±6	20±5
$pK^o\overline{K^o}\pi^{\pm}$	56±7	64±7
$\Lambda K^+\pi^o\pi^{\pm}$	103±13	121±11
$\Lambda K^o\pi^+\pi^{\pm}$	122±14	62±9
$\Sigma^oK^o\pi^+\pi^{\pm}$	38±11	23±6
$\Sigma^+K^o\pi^o\pi^{\pm}$	34±9	66±14
$\Sigma^+K^+\pi^-\pi^{\pm}$	24±6	118±17
$\Sigma^-K^+\pi^+\pi^{\pm}$	20±4	19±4
$pK^oK^{\pm}$	80±13	70±8

IV. RESONANCE PRODUCTION

In this section, we compute the cross sections for the resonant final states,

$$\Sigma^+K^*(890)^+ \quad , \tag{13}$$

and

$$\Sigma(1385)^+K^+ \quad . \tag{14}$$

Reactions ii and iv of Table I are used for (13) and (14) respectively. We also look at the resonant production in reactions vi, vii, and viii of Table I. The remainder of the reactions in Table I are not pursued further either because of statistics, resolution or ambiguities, or some combination of these reasons. For reaction vii, we have used events from the entire restricted sample.

A. $\Sigma^+K^*(890)^+$ and $\Sigma(1385)^+K^+$

For the final states (13) and (14), we fit the appropriate Dalitz plot to determine the fraction of resonant production present. For (13), we choose the Dalitz plot for reaction ii of Table I, using only those events where the K^o is visible. For (14), we choose the Dalitz plot for reaction iv, again where the Λ is visible. In both cases, there is only one prominent resonance in the final state, namely, the one of interest. There is the possibility of the presence of N^* or Δ which can decay into (ΛK) or (ΣK), but these resonances are generally both broad and weakly coupled to these decay channels. Therefore we do not consider them any further for the final states (13) and (14).

The fitting procedure is analogous to the simple non-interference model used by Bland et al.[9] Our formulae are less complicated since we consider only one resonance, whereas Ref. 9 must be concerned with two crossing resonant bands. Moreover, we omit the angular momentum barrier factor since we are at a much higher incident momentum and therefore have many partial waves present in the interaction.

We number the stable particles in the final state 1, 2, and 3 with the resonance occurring in the combination (1,2). Let:

m_{12} = invariant mass of particles 1 and 2

m_{23} = invariant mass of particles 2 and 3

Then we can write:

$$\frac{d^2\sigma}{dm_{12}^2\, dm_{23}^2} = a + bI_{12} \tag{15}$$

where $I_{12} = (BW)\cdot(1 + A\cos^2\lambda)$, (16)

$$(BW) = \frac{1}{\pi}\frac{m_o\Gamma\cdot(\frac{p_o}{p})}{(m_{12}^2 - m_o^2)^2 + (m_o\Gamma)^2}, \tag{17}$$

$$\Gamma = \Gamma_o\left(\frac{p^2}{p^2 + X^2}\Big/\frac{p_o^2}{p_o^2 + X^2}\right)\frac{p}{p_o}, \tag{18}$$

λ = decay angle in the (1,2) center of mass with respect to particle 3,

m_o; Γ_o = mass, width of the resonance,

p = momentum of particle 1 (or 2) in the (1,2) center of mass,

p_o = value of p when $m_{12} = m_o$, and

X = inverse radius of interaction.

This description of the resonance is basically that discussed by Jackson,[10] where the fact that we are dealing with p-wave resonant behavior has been taken into account. The values for m_o and Γ_o are taken from the Particle Data Tables,[6] and are as follows:

For $K^*(890)^+$, m_o = 891 MeV, Γ_o = 50 MeV

For $\Sigma(1385)^+$, m_o = 1382 MeV, Γ_o = 36 MeV.

The inverse radius of interaction, X, is taken to be the pion mass. The parameters a, b, and A are to be determined by the fit, with the overall normalization constrained to give the total cross section as determined in Sec. III.

The factor $1 + A \cos^2 \lambda$ describes the most general behavior a p-wave resonance can have as the Dalitz plot is traversed parallel to the resonance band. However due to the meager statistics, our data are not very sensitive to the parameter A. Since the fitting for A gives an answer with large errors which is consistent with zero, we omit this factor by setting $A = 0$.

Figure 5 shows the Dalitz plot for reaction ii of Table I and Fig. 6 shows the distribution of the K-π mass. It is clear that this final state is dominated by (13). The results of the fit are given in Table IX. To get the total cross section, we note that the $K^*(890)$ decays into $K\pi$ only,[6] and calculate from Clebsch-Gordan coefficients that

$$\frac{K^*(890)^+ \rightarrow K^o\pi^+}{K^*(890)^+ \rightarrow K^+\pi^o} = \frac{2}{1} \quad .$$

Table IX.

Final state	No. events used in fit	χ^2	d.f.	% of channel	Cross section incl. all decay channels
$\Sigma^+K^*(890)^+$	48	7.6	7	63±7	98±20 μb
$\Sigma(1385)^+K^+$	239	13.8	11	26±4	28±5 μb

Figure 7 shows the Dalitz plot for reaction iv of Table I and Fig. 8 shows the distribution of the Λ-π mass. The results of the fit are given in Table IX. The branching fraction for $\Sigma(1385) \rightarrow \Lambda\pi$ is taken to be 0.9 from the Particle Data Tables.[6]

B. $pK^+\overline{K^o}$

Reaction vi of Table I does not have as distinctive a structure as the ones discussed in the preceding section. The only clearly discernible resonant state is the A_2 meson. Figure 9 shows the Dalitz plot for reaction vi and Fig. 10 shows the distribution of the $K^+\overline{K^o}$ mass. There is perhaps a hint of a bump near 1560 MeV in the $K^+\overline{K^o}$ mass but it is not statistically compelling.

The final state pA_2 has become the object of intensive study recently because of the discovery of the A_2 splitting.[11] While Fig. 10 does not have enough events to show the splitting, it does have a feature similar to that reported by Crennell et al.[12] The $K\overline{K}$ decay appears to give only the "high side" of the A_2 (A_{2H}); the center of the peak is about 1320 MeV. However, there still seems to be an excess of events in the region of the "low side" of the A_2 (A_{2L}). Evidence from a $p\overline{p}$ experiment[13] and from a recent missing mass spectrometer experiment[14] shows that the $K\overline{K}$ decay comes from both sides of the A_2.

We do not fit this region for A_2 production because of the uncertainty in the shape. However, we can crudely estimate its production. If we estimate the background to be about 2 events per 25 MeV from 1250 to 1350, we see an excess of about 17 events. This number corresponds to a partial cross section for $\pi^+p \rightarrow pA_2^+$ (where only $A_2^+ \rightarrow K^+\overline{K^o}$ is included) of $\frac{17}{92} \times 70\ \mu b \doteq 13\ \mu b$. The greatest error in this estimate is the uncertainty in the shape of the A_2. We assign the error to be 6 μb. A more interesting number is the branching fraction for $A_2 \rightarrow K\overline{K}$. In this experiment, the cross section for $\pi^+p \rightarrow pA_2$ is[15] (310±80) μb, where the A_2 decays either to $\rho\pi$ including both $\rho^+\pi^o$ and $\rho^o\pi^+$, or to $\eta\pi^+$

including both neutral and charged decay modes of the η. Combining these two cross sections gives the branching fraction:

$$\frac{A_2^+ \rightarrow K^+\overline{K^o}}{A_2^+ \rightarrow \text{all}} = 0.04 \pm 0.02 \quad .$$

This result compares favorably with the world average[6] which is 0.024± 0.005.

C. $p\pi^+K\bar{K}$

We observe the $p\pi^+K\bar{K}$ channel via the following final states:

$$p\pi^+K^+K^- \ , \tag{19}$$

$$p\pi^+K_1^oK_1^o \ , \tag{20}$$

and

$$p\pi^+K_1^oK_2^o \quad . \tag{21}$$

In the final state (20), we may see one or both vees, while in (21) we can only see one vee. All three final states exhibit a good deal of structure. Discernible features include $\Delta(1236)^{++}$, $K^*(890)$, $\varphi(1019)$, f(1260) and A_2 production. Table X summarizes the resonance production in these final states. Determination of the production rates is discussed below.

Table X.

Final state	Final state used	Cross section μb including all decay channels
$\Delta(1236)^{++}\ K^+K^-$	$p\pi^+K^+K^-$	36±7 μb
$pK^+\overline{K^*}(890)^o$	$p\pi^+K^+K^-$	23±5
$\Lambda(1520)\ \pi^+K^+$	$p\pi^+K^+K^-$	16±6
$p\pi^+\ \varphi(1019)$	$p\pi^+K^+K^-$	10±3
$\Delta(1236)^{++}\ \varphi(1019)$	$p\pi^+K^+K^-$	< 2
$\Delta(1236)^{++}\ K_1^oK_1^o$	$p\pi^+K_cK_c$	11±5 μb
$\Delta(1236)^{++}\ K_1^oK_2^o$	appropriate difference between $p\pi^+K_cK_n$ and $p\pi^+K_cK_c$	small; see text
$pK^o\ K^*(890)^+$	appropriate sum of $p\pi^+K_cK_n$ and $p\pi^+K_cK_c$	29±10

1. $p\pi^+K^+K^-$

Figure 11 shows a triangle plot for the final state (19). The $\Delta(1236)^{++}$ and the $\varphi(1019)$ are clearly visible. Less obvious are the A_2^o and the f(1260). Figure 12 shows a plot of the $p\pi^+$ mass where again the prominence of the $\Delta(1236)^{++}$ is obvious. Figure 13 is a plot of the K^+K^- mass. Here the $\varphi(1019)$ is clearly seen. The broad enhancement from about 1175 MeV to 1350 MeV comes from the f(1260) and A_2^o which overlap because of their broad (effective) widths. Figure 14 displays the mass of the K^+K^- when the $p\pi^+$ mass is in the Δ^{++} band. Figure 15 shows the π^+K^- mass spectrum, where the $K^*(890)^+$ is a prominent feature. Finally, Fig. 16 shows the pK^- mass spectrum in which the $\Lambda(1520)$ is visible.

Because of the complexity of this final state, we do not try to fit for all the resonance production. In particular, we make no attempt to untangle the A_2^o and f(1260) production. For these two resonances, even resolving their production in association with a Δ^{++} is difficult, as is illustrated by the following numbers. The cross section for $\pi^+p \to \Delta^{++} A_2^o$ is (90±20) μb[16] where only the decay mode $A_2^o \to \pi^+\pi^-\pi^o$ (no ρ selection) is included. Using 0.23±0.08 as the branching fraction[15] for $A_2^o \to \eta\pi^o$ and 0.024±0.005 as the branching fraction[6] for $A_2^o \to (K\bar{K})^o$, we predict 12±4 events for $A_2^o \to K\bar{K}$. Since there can be interference between the f and the A_2^o, these events can appear on the K^+K^- and $K^o\overline{K^o}$ mass plots in any ratio (not just 1 to 1 as for pure A_2^o). Figure 14 shows on the order of 20 events above background in this mass region. Since the cross section for $\pi^+p \to \Delta^{++}f(1260)$ is (160±40) μb,[17] about all we can say is that the branching fraction for f(1260) into $K\bar{K}$ must of the same order of magnitude as the branching fraction for $A_2^o \to K\bar{K}$.

To get the $\Delta(1236)^{++}$ contribution, we fit the $p\pi^+$ mass distribution (Fig. 12) for the resonance plus phase space. In doing this fit, we are averaging over all the other structure including interference (if there is any). The justification is essentially pragmatical in the sense that the distribution appears to be structureless except for the Δ^{++}. However, the chi-square (25.7 for 20 degrees of freedom, corresponding to a confidence level of about 20%) for the fit is not very good, and for that reason we enlarge the error on the result by a factor $\sqrt{2}$. The main contribution to the chi-square comes from the narrow observed width of the Δ^{++}.

To get the contribution for the $K^*(890)^o$, we follow the above procedure for the π^+K^- mass distribution (Fig. 15). The chi-square for the fit is 18 for 18 degrees of freedom. In the K^* cross section, we include the branching fraction correction for decay into $K^o\pi^o$. For other resonance states, we only try to estimate their production.

To estimate the $\Lambda(1520)$ production we use the pK^- mass region in Fig. 16 from 1500 MeV to 1550 MeV, which has 50 events. To estimate the background, we average the bin just above this region with the bin just below it. This averaging gives 21±5 events for the background. However, the statistical error for this estimate does not reflect the true uncertainty in the background. For this reason, we multiply the statistical error by $\sqrt{2}$. Using the total cross section from Table VII and the branching fraction of 0.45 from the Particle Data Tables,[6] we obtain the cross section for $\pi^+p \rightarrow \Lambda(1520)\pi^+K^+$:

$$\sigma(\pi^+p \rightarrow \Lambda(1520)\pi^+K^+) = (16\pm6)\ \mu b \qquad \text{(all decay modes)} \qquad (22)$$

The narrow $\varphi(1019)$ appears as part of the K^+K^- spectrum (Fig. 13). The only complication in estimating its production comes from a rapidly rising background from the well-known "s-wave" enhancement, seen in a previous study of this reaction.[18] The inset in Fig. 13 shows the φ region of the K^+K^- mass spectrum, plotted in 4 MeV bins and centered so that the central value (1019.5 MeV) of the φ coincides with the center of the bin. To estimate the production rate we use the five bins surrounding 1019.5 MeV which contain a total of 27 events. We estimate the background by drawing various straight lines through the neighboring regions; the result for the background is 8±2 events. Using the total cross section of (80±8) μb from Table VII, and the branching fraction of 0.48±0.02 for the Particle Data Tables,[6] we obtain the cross section for $\pi^+p \rightarrow p\pi^+\varphi$:

$$\sigma(\pi^+p \rightarrow p\pi^+\varphi) = (10\pm3)\ \mu b \qquad \text{(all decay modes)} \qquad (23)$$

A final number of interest is the production of the quasi-two-body final state $\Delta(1236)^{++}\ \varphi(1019)$. Figure 17 shows the $p\pi^+$ mass spectrum for the 27 events which are inside the φ region in K^+K^- mass (we use the five bins used for the φ cross section). The $p\pi^+$ spectrum below 1350 MeV, which includes practically all of the Δ^{++}, contains 6 events. If we assume that the spectrum above 1350 MeV is given by phase space for the final state $p\pi^+\varphi$, we predict that there should be 9 events below 1350 MeV. Included in this prediction is the assumption that the background is distributed in the same way as the $p\pi^+\varphi$ events. However, if we use the above calculation for the background and make the extreme assumption that all eight background events fall above 1350 MeV, we still predict 6 events below 1350 MeV. Thus our result is certainly consistent with no $\Delta^{++}\varphi$ production. The best we can do is set an upper limit.

We assume a binomial distribution for the two parts of the $p\pi^+$ spectrum below and above 1350 MeV. We further assume that 100% of the $\Delta(1236)^{++}$ is below 1350 MeV. The relative amount of resonance and phase space is a free parameter in the distribution. We choose the one-sided 90% confidence limit by finding the value of the parameter which decreases the likelihood function to $e^{-0.79}$ of its maximum likelihood value. The two background assumptions discussed above give one event and 4.6 events respectively. We take the larger of the two numbers and state:

$$\sigma(\pi^+ p \rightarrow \Delta^{++}\varphi) \leq 2\ \mu b \quad . \tag{24}$$

If this limit were the actual value of the cross section, the probability of obtaining our result would be 8%.

The suppression of this channel is certainly one of the prominent features of these data. We will return to discuss this result in the section on physical characteristics.

2. $\underline{p\pi^+K^o\overline{K^o}}$

This final state occurs either as the state (20) or the state (21). We actually observe events with two vee's and events with one vee. The events with two vee's are all from (20) while those with one vee are from both (20) and (21). In order to extract information about the final state (21), we must perform a subtraction of the two sets of events. If there were no escape corrections and if the branching fraction for $K_1 \rightarrow \pi^+\pi^-$ were exactly 2/3, then the final state (20) would contribute equally to the two classes of observed events. With the escape corrections and real branching fraction, the actual contributions are slightly different.

The difference between these final states is quite remarkable. The final state (20) has a strong $\Delta(1236)^{++}$. However, within the small statistics, it does not seem to have any particularly prominent $K_1^oK_1^o$ structure. There seems to be some departure from phase space in the pK^o spectrum, but it is not consistent with the known Y_1^* resonances. In contrast, the final state (21) has practically no $\Delta(1236)^{++}$. As is well known, the $\varphi(1019)$ appears in the $K_1^oK_2^o$ spectrum, but any other structure is difficult to discern. The above statement about the pK^o spectrum applies to this final state also.

The phi production in (21) is consistent with that from the final state (19). From the Particle Data Tables,[6] we find the ratio of the branching fractions for

$$\frac{\varphi \rightarrow K^+K^-}{\varphi \rightarrow K_1^oK_2^o} = \frac{(45.5\pm3.3)}{(36.4\pm3.4)} = 1.25\pm0.15 \ .$$

Since we see 19±6 events from (19), we expect $(0.68\pm0.01)(19\pm6)/(1.25\pm0.15)$ = 10±3 events in the final state (21) with visible K_1^o. From Fig. 20 we estimate that there are 11±4 events in the φ peak. These differences are displayed in Figs. 18 to 21. In each figure, part (a) shows the spectrum from events with two vees, part (b) shows the spectrum from events with one vee, and part (c) shows the appropriate subtraction that corresponds to the pure final state (21). Figure 18 shows the $p\pi^+$ spectrum; Fig. 19, the π^+K^o spectrum; Fig. 20, the $K^o\overline{K^o}$ spectrum; and Fig. 21, the pK^o spectrum. In Figs. 19 and 21, each event is plotted twice.

As in the case of final state (19), we fit for the $\Delta(1236)^{++}$ and $K^*(890)^+$. For the Δ^{++}, we find a (50±20)% contribution in final state (20), while fitting the subtracted data from Fig. 18c gives a negative

percentage for the Δ^{++} contribution to final state (21). To test the significance of the difference of these two numbers, we have performed simultaneous fits to the final states (20) and (21), first demanding the percentage of Δ^{++} be the same in both states, and then allowing the percentages to be different. For the case demanding the same percentage, we obtain a chi-square of 11.0 and a common percentage of (14±8)%. For the second case we find a chi-square of 7.7 with the result stated above for final state (20) and (- 16±18)% for the final state (21). Thus the difference corresponds to about a two standard deviation effect.

At this point we note that any K^* contribution can come only from the π^+K^o combination since the $\pi^+\overline{K^o}$ combination must have an isospin of 3/2. Since the K^* seems to be in both final states (20) and (21), we add the two distributions shown in Fig. 19a and 19b with weights appropriate to give the distribution corresponding to the total $p\pi^+K^o\overline{K^o}$. The addition is roughly twice Fig. 19a plus Fig. 19b. We find that the K^* contribution to the total final state is (30±10)%, with a chi-square of 15 for 14 degrees of freedom.

V. SOME PHYSICAL CHARACTERISTICS OF THE DATA

In this section we discuss some physical characteristics of reaction i of Table I and the final states (14), (19), (20), and (21). For the two-body states, we compare the t distribution for the corresponding crossed reactions from K^-p experiments. This comparison has interest in connection with the concept of "line reversal."[19] For the four-body states, the discussion centers on the suppression of the Δ^{++} in some of the final states.

A. Σ^+K^+ t Distribution

Figure 22 shows the Σ^+K^+ t distribution and the fit to the initial slope. We find for the slope the value (8.4 ± 1.4) $(\mathrm{GeV/c})^{-2}$. The range of t over which the fit is performed is 0.02 $(\mathrm{GeV/c})^2$ to 0.4 $(\mathrm{GeV/c})^2$ where the beginning value corresponds to the kinematic limit. The chi-square for the fit is 0.9 for 5 degrees of freedom.

This value for the slope of the t distribution is very similar to the slope of the π^+p elastic scattering t distribution near this energy. It is also similar to the slope of the t distribution for $K^-p \rightarrow \Sigma^+\pi^-$ at about 4.1 GeV/c incident momentum.[20] If we extrapolate our slope to t = 0, we obtain an intercept that also agrees very well with the intercept from the K^-p experiment[20] when we scale their intercept to our momentum. We scale their intercept by $(P_{lab})^{-n}$ using their value of $n = 1.8\pm0.4$, where P_{lab} is the momentum of the incident K^-. Table XI shows this comparison. This agreement has been pointed out before.[19]

Table XI. Comparison of $\pi^+p \rightarrow \Sigma^+K^+$ at 3.7 GeV/c with $K^-p \rightarrow \Sigma^+\pi^-$ at 4.1 GeV/c. The intercept from the K^- experiment is scaled as discussed in the text.

	Slope, $(\mathrm{GeV/c})^{-2}$	$\left.\frac{d\sigma}{dt}\right\|_0$, $\frac{\mathrm{mb}}{(\mathrm{GeV/c})^2}$
$\pi^+p \rightarrow \Sigma^+K^+$	8.4 ± 1.4	0.69 ± 0.16
$K^-p \rightarrow \Sigma^+\pi^-$ (Ref. 20)	7.3 ± 1.3	0.80 ± 0.25

We also note the backward peak in the distribution which corresponds to hyperon exchange.

B. $\Sigma(1385)^+K^+$ t and Decay Distributions

Figure 23 shows the distribution of $t' = |t| - |t|_{min}$ for the reaction $\pi^+p \rightarrow \Sigma(1385)^+K^+$. We plot t' instead of t to emphasize that the turnover in the forward direction is not kinematical. We fit for the slope, omitting the first point, over the range $0.12\ (GeV/c)^2 \leq t' \leq 1.5\ (GeV/c)^2$. The slope so obtained is $(3.0\pm0.6)\ (GeV/c)^{-2}$. The chi-square for this fit is 0.32 for 2 degrees of freedom. Including the first point gives a slope of $(2.5\pm0.4)\ (GeV/c)^{-2}$ with a chi-square of 2.8 for 3 degrees of freedom. Obviously, either value is acceptable.

Although the turnover could be statistical rather than dynamical, we prefer the latter interpretation. In the 8 GeV/c π^+p experiment,[7] the corresponding t distribution shows a hint of this effect, with even poorer statistics, and their value of the slope is lower, although not inconsistent with ours. Furthermore, in other K^-p experiments at 3.5 GeV/c[21] and 4.1 GeV/c,[22] t distributions for $K^-p \rightarrow \Sigma(1385)^+\pi^-$ show hints of a turnover near $t = 0$. For these reasons we prefer the first value mentioned for the slope of our data and that slope is the one plotted in Fig. 23. Reference 21 does not fit their angular distribution. Reference 22 fits the sum of their 4.1-GeV/c and 5.5-GeV/c data and finds a value similar to ours. Table XII shows the comparison of slopes for the various experiments mentioned above.

Table XII. Comparison of slopes of t distribution.

Reaction	Incident momentum GeV/c	Slope $(GeV/c)^{-2}$
$\pi^+p \rightarrow \Sigma(1385)^+K^+$	3.7	3.0±0.6
$\pi^+p \rightarrow \Sigma(1385)^+K^+$	8	1.9±0.9
$K^-p \rightarrow \Sigma(1385)^+\pi^-$	4.1 and 5.5	2.7±0.4

Figure 24 shows the decay distributions for this reaction. Figure 24a is the $\cos(\alpha)$ distribution and Fig. 24b is the φ distribution. The curves on these histograms are the predictions of the Stodolsky-Sakurai model.[23] The agreement with the model is good, which is also the result of Ref. 22 for $K^- p \to \Sigma(1385)^+ \pi^-$.

C. $\pi^+ p \to \Delta^{++} \varphi$ and SU_3

In the previous section, we have noted the suppression of the final state $\Delta^{++}\varphi$. In the framework of SU_3 or the quark model, the φ meson is related to the ω meson in that these two physical states are "mixtures" of two SU_3 "pure" states. We use the value[24] (0.66 ± 0.08) μb for the $\pi^+ p \to \Delta^{++}\omega$ cross section to obtain the ratio of cross sections:

$$\rho = \frac{\sigma(\pi^+ p \to \Delta^{++}\varphi)}{\sigma(\pi^+ p \to \Delta^{++}\omega)} \leq \frac{1}{330}$$

where the confidence limit is the same as for Eq. (24). At our momentum, the center-of-mass momenta are 0.83 GeV/c and 0.96 GeV/c for the $\Delta\varphi$ and $\Delta\omega$ states respectively. Thus for this comparison, the phase space corrections are small, and we neglect them. In passing, we note that the ratio ρ is consistent with the squared coupling constant ratio, $g^2_{\varphi\rho\pi}/g^2_{\omega\rho\pi} \doteq 1/600$ as determined collectively from the experimental φ and ω widths, the $\varphi \to \rho\pi$ branching fraction, and the ratio of available phase space for $\varphi \to \rho\pi$ and $\omega \to \rho\pi$.[25]

In the framework of the quark model, a zero value for ρ means that the φ is entirely $\lambda\bar{\lambda}$ and the ω is entirely $n\bar{n} + p\bar{p}$. If we denote the φ-ω mixing angle by θ, this angle θ can be related to ρ in the following way[26]:

$$\pm\sqrt{\rho} = \frac{\langle \pi^+ p | \Delta^{++} \varphi \rangle}{\langle \pi^+ p | \Delta^{++} \omega \rangle} = \tan(\theta_o - \theta)$$

where $\theta_o = \arctan(1/\sqrt{2}) \doteq 35.26^o$. This relationship gives a model-dependent determination of the mixing angle, but in a way that is independent of the meson masses in the 1^- nonet. We find $|\theta_o - \theta| \leqq 3.15^o$, or:

$$32.1^o \leqq \theta \leqq 38.4^o$$

where the interval corresponds to the confidence limit of Eq. (24).

In principle, this approach could yield information about whether the linear or quadratic form of the Gell-Mann/Okubo mass formula is appropriate for bosons. In practice, however, the values are sufficiently close ($|\theta(\text{linear})| = 37.1^o \pm 1.1^o$; $|\theta(\text{quadratic})| = 39.9^o \pm 1.1^o$) that our data do not distinguish clearly between them, although the linear value is favored. In any case, the final conclusion would rest on the validity of this quark model.[26]

D. Suppression of Other States in $p\pi^+K\bar{K}$

The result discussed in the previous paragraph is part of a more general picture that appears when we consider together the three final states (19) through (21). We have seen that the $\Delta(1236)^{++}$ is very prominent in $p\pi^+K_1^oK_1^o$ and practically non-existent in $p\pi^+K_1^oK_2^o$. This observation leads us to conjecture that perhaps the quantum numbers of the K-$\bar{K}$ system are restricted when it is produced in conjunction with a Δ. Since the φ decays to $K_1^oK_2^o$ and not to $K_1^oK_1^o$, it would have the wrong set of quantum numbers to go with a Δ, which is consistent with the result expressed by Eq. (24).

Both $K_1^oK_1^o$ and $K_1^oK_2^o$ are CP eigenstates with CP = + 1 since for a two boson system, the charge conjugation, $C = (-1)^\ell$, and the parity, $P = (-1)^\ell$ also, where ℓ = orbital angular momentum quantum number. Since K_1^o and K_2^o are CP eigenstates with opposite CP values, the angular momentum for $K_1^oK_1^o$ must be even and that for $K_1^oK_2^o$ must be odd. This difference leads to states of opposite parity (and charge conjugation). Thus we conclude that the K-$\bar{K}$ system can be produced with the Δ^{++} only if that system has even parity.

If we take the final state $\Delta^{++}K^+K^-$ and look at the center of mass of the K^+K^- (the "Jackson frame"), we find that the distribution of $\cos(\alpha)$ is forward-backward symmetric. The angle α is the angle of the K^+ with respect to the incident π^+ in the Jackson frame. Figure 25 shows the $\cos(\alpha)$ distribution for those events which have a $p\pi^+$ mass in the Δ^{++} mass region. Figure 26 shows the $\cos(\alpha)$ distribution for the $p\pi^+K^+K^-$ where the Δ region (1160 MeV to 1280 MeV) has been omitted. The symmetry of the $\cos(\alpha)$ distribution for $\Delta^{++}K^+K^-$ is consistent with the above conclusion in that states of single parity cannot combine to give a forward-backward asymmetry. Furthermore, the $\cos(\alpha)$ distribution for the complementary set of events does not show such symmetry. The striking characteristic of Fig. 25 is that the distribution is integrated over the total K^+-K^- spectrum and still shows the symmetry.

Finally, we note that Fig. 14 shows no evidence for the $K\bar{K}$ s-wave threshold enhancement in the final state $\Delta^{++}K^+K^-$. However, the enhancement is clearly present in the overall final state $p\pi^+K^+K^-$, as Fig. 13 indicates.

VI. SUMMATION

For the π^+p interaction, we have presented both stable particle and resonant production cross sections for the major strange particle final states. Tables VII, IX, and X summarize these results. In addition, we estimate the total cross section for strange particle production is about 1.5 mb. Although it is not mentioned above, we see no evidence for a new 1480 MeV Λ-π resonance[27] (see Fig. 8).

To test the concept of line reversal, we have compared $\pi^+p \rightarrow \Sigma^+K^+$ with $K^-p \rightarrow \Sigma^+\pi^-$ and $\pi^+p \rightarrow \Sigma(1385)^+K^+$ with $K^-p \rightarrow \Sigma(1385)^+\pi^-$, where the comparison in each case involves the momentum transfer distributions. The agreement in each case is good.

We have studied the $p\pi^+K\bar{K}$ final state in some detail and obtain the following results: (a) While the final state $p\pi^+\varphi$ is clearly present, our data set an upper limit for $\Delta^{++}\varphi$ production of 2 μb. (b) The Δ^{++} and the $K^*(890)$ are prominent features in the final state $p\pi^+K\bar{K}$. (c) The $K\bar{K}$ state occurring with the Δ^{++} is either $K_1^oK_1^o$ or K^+K^- in even parity angular momentum states. However no threshold enhancement is associated with the Δ^{++}.

ACKNOWLEDGMENTS

This thesis represents the materialization of many years of encouragement and help from relatives and friends. Since space does not permit personal mention of everyone, I simply thank God for blessing me with so many kind and generous associates.

I wish to thank all of the members of the Trilling-Goldhaber Group, including the scanning and programming staffs, for all the assistance and encouragement they have supplied. Special thanks go to Mrs. Belinda Sieh and Mrs. Irene Witkowski for special scanning tasks well done and to Harriett Rice and Mrs. Bronwyn Hall for help with the figures. It is difficult to adequately express my gratitude to my colleagues, Jimmy MacNaughton and Don Coyne, from whom I have learned a great deal. To my advisor and teacher, Professor George Trilling, goes my lasting admiration for his guidance, inspiration, patience and understanding which he has shown to me as his student.

I wish to acknowledge support from David Lipscomb College, the National Science Foundation and the Atomic Energy Commission.

To my wife, Judy, and my sons, Jonathan and Stephen, I dedicate this thesis.

APPENDIX

Normalization Calculation

Here we apply the philosophy of Section III-B to calculate the microbarn equivalents for the regions of film considered. To facilitate the discussion, the following subscripts are used to designate different regions of film:

p means proton film

1 means film in which all events are fully processed

2 means film in which all events are recorded but only the first measurement is available for ordinary events

3 means film in which not all events are recorded

4 means total pion film, i.e., regions 1, 2, and 3.

Because we have only the first measurement for regions 2 and 3, we need an additional assumption in order to determine the proton contamination in these regions. For this purpose, we assume that the scanning, measuring, and fitting procedures treat pion-induced and proton-induced four-prong events with equal efficiency. We will refer to this assumption as "the equality assumption." This assumption is true only for events which satisfy the fiducial volume and beam track criteria. We will therefore account for the outside fiducial volume rejects and the non-beam rejects before applying the above assumption.

Before we begin, we define the symbols we will need in the formulae we use:

A = total number of acceptable events due to incident pions

B = total number of four prongs recorded due to incident pions inside fiducial volume

C = total number of four prongs recorded due to incident protons inside fiducial volume

E_1 = number pion events lost due to small angle elastic scatters

F = total number four-prong events accepted

G = total number four-prong events accepted due to incident pions

H = total number four-prong events accepted due to incident protons

J = total number four-prong events rejected for outside fiducial volume or non-beam track

m = microbarn equivalent for interactions due to pions

S = total number four-prong events recorded

T = total number accepted events

U = total number unique $pp \rightarrow pp\pi^+\pi^-$ events accepted

V = total number unique $\pi^+p \rightarrow p\pi^+\pi^+\pi^-$ events accepted

X = number unique $pp \rightarrow pp\pi^+\pi^-$ after first measurement

Y = number unique $\pi^+p \rightarrow p\pi^+\pi^+\pi^-$ after first measurement

σ_o = total π^+p cross section at our momentum; the value used is 28100 microbarns

The quantity E_1 is needed only for region 1, thus the presence of the subscript. The value of E_1 is determined by fitting the momentum transfer distribution for elastic scattering to a function for e^{bt}, where t is the momentum transfer and b is a parameter to be determined. The fitting procedure is performed over an interval of t where losses are not strongly dependent on t. The loss E_1 is found by integrating the function over the region of small t to get the total number of events expected and subtracting the number of events found. We obtain the value:

$$E_1 = 1328 \pm 119 \text{ events} \tag{A1}$$

The quantities A, B, C, E_1, G, H, m and σ_o are calculated quantities; the rest are measured by counting events. Table I-A gives the values of the measured quantities that we need to calculate the others.

We deal first with region 1. Of immediate interest is the quantity A, which we use to calculate m_1, the microbarn equivalent for region 1:

$$A_1 = T_1 - T_p \cdot U_1/U_p + E_1 \tag{A2}$$

Table I-A. Event totals used for normalization calculation. Symbols are explained in the text.

Region →	p	1	2	3
Quantity ↓				
F	245	13907	--	--
J	21	2837	--	--
S	281	18490	5238	32605
T	1613	43993	--	--
U	122	442	--	--
V	0	4823	--	--
X	--	--	66	569
Y	--	--	983	5865

$$m_1 = \sigma_o/A_1 \quad . \tag{A3}$$

For the calculation in regions 2 and 3, we will also need:

$$B_1 = (S_1 - J_1) - (S_p - J_p) \cdot U_1/U_p \tag{A4}$$

$$G_1 = F_1 - F_p \cdot U_1/U_p \quad . \tag{A5}$$

For regions 2 and 3, we use the equality assumption to write:

$$\frac{C_i}{B_i} = \frac{H_i}{G_i} \quad ; \quad i = 2, 3 \quad . \tag{A6}$$

We rearrange this equation to obtain:

$$\frac{C_i}{B_i} = \frac{H_i}{U_i} \cdot \frac{U_i}{V_i} \cdot \frac{V_i}{G_i} \quad . \tag{A7}$$

Further appeal to the equality assumption allows us to write:

$$U_i/V_i = X_i/Y_i \quad . \tag{A8}$$

The ratio H/U is a physical property of proton-proton interactions and is therefore calculated using the results from the proton film:

$$\frac{H_i}{U_i} = \frac{F_p}{U_p} \quad . \tag{A9}$$

($F_p = H_p$ since, by assumption, there are no pions in the proton film.)

Likewise the ratio V_i/G_i is a physical property of pion-proton interaction and is calculated from the quantities of region 1 where the proton subtraction is made directly.

$$\frac{V_i}{G_i} = \frac{V_1}{G_1} \quad . \tag{A10}$$

Substituting Eqs. (A8), (A9), and (A10) into Eq. (A7) and solving for C_i gives:

$$C_i = B_i \cdot \frac{F_p}{U_p} \cdot \frac{X_i}{Y_i} \cdot \frac{V_1}{G_1} \quad . \tag{A11}$$

From the definitions, we can write:

$$S_i = B_i + C_i + J_i \quad . \tag{A12}$$

We assume the reject rate is the same for all regions of the pion film:

$$J_i = S_i \cdot J_1/S_1 \quad . \tag{A13}$$

Substituting (A11) into (A12) and solving for B_i gives:

$$B_i = S_i \cdot \frac{(S_1 - J_1)}{S_1} \cdot \left[1 + \frac{F_p}{U_p} \cdot \frac{X_i}{Y_i} \cdot \frac{V_1}{G_1}\right]^{-1} \quad . \tag{A14}$$

From Eq. (A14), we can see that the only measured quantities needed from region i (= 2,3) are S_i, X_i and Y_i.

We may now determine the (expected) numbers of acceptable events and the corresponding microbarn equivalent:

$$A_i = B_i \cdot A_1/B_1 \tag{A15}$$

$$m = \sigma_o/A_i \quad . \tag{A16}$$

The total number of acceptable events is given by:

$$A_4 = A_1 + A_2 + A_3 \tag{A17}$$

and the microbarn equivalent by:

$$m_4 = \sigma_o/A_4 \quad . \tag{A18}$$

As an alternative, we could use

$$m_4^{-1} = m_1^{-1} + m_2^{-1} + m_3^{-1} \quad , \tag{A19}$$

which is just a disguised way of writing Eq. (A17). Table II-A summarizes the calculations for regions 1, 2, and 3 by giving total acceptable events, acceptable pion events, and their difference.

In Table IV of Section III, we quote for the region "All events recorded," which is the sum of what we have here called regions 1 and 2. This number is obtained from the formula analogous to Eq. (A19).

The errors in each calculated quantity is determined by computing the changes in the quantity when each independent variable, one at a time, is changed by the amount of its error. Then the changes due to each independent variable are added in quadrature, and the square root of the result is the error on the quantity considered. Except for the error on E_1, only statistical errors are considered.

Table II-A. Summary of effects of proton contamination.

	Region	1	2	3
T^*	Total acceptable events	45321±241	11900±230	74071±1084
A	Acceptable pion events	39477±623	11333±243	69084±1191
(T^*-A)	Acceptable proton events	5844±585	566±77	4986±367

*Includes the elastic scattering correction

REFERENCES

1. W. Chinowsky, R. R. Kinsey, S. L. Klein, M. Mandelkern, J. Schulz, F. Martin, M. L. Perl, and T. H. Tau, Phys. Rev. 165, 1466 (1968); David Gordon Brown, π^+p 4-prong Interactions Between 3 and 4 GeV/c, UCRL-18254 (Ph.D. Thesis), 1968 (unpublished).
2. Alvarez Group Program Note P-117 (unpublished).
3. Alvarez Group Program Note P-126 (unpublished).
4. G. Alexander, O. Benary, and U. Maor, Nucl. Phys. B5, 1 (1968).
5. A. Citron, W. Galbraith, T. F. Kycia, B. A. Leontic, R. H. Phillips, A. Rousset, and P. H. Sharp, Phys. Rev. 144, 1101 (1966).
6. Particle Data Group, Rev. Mod. Phys. 41, 109 (1969); 42, 87 (1970).
7. Aderholz et al., Nucl. Phys. B11, 259 (1970).
8. O. I. Dahl, L. M. Hardy, R. I. Hess, J. Kirz, and D. H. Miller, Phys. Rev. 163, 1377 (1967).
9. Bland et al., Nucl. Phys. B13, 595 (1969).
10. J. D. Jackson, Nuovo Cimento 34, 1644 (1964).
11. Chikovani et al., Phys. Letters 28B, 233 (1968).
12. D. J. Crennell, U. Karshon, K. W. Lai, J. M. Scarr, and I. O. Skillicorn, Phys. Rev. Letters 20, 1318 (1968).
13. Aguilar-Benitez et al., Phys. Letters 29B, 62 (1969).
14. Baud et al., Phys. Letters 31B, 397 (1970).
15. Donald G. Coyne, private communication.
16. Keith W. J. Barnham, private communication.
17. Bronwyn H. Hall, private communication.
18. G. H. Trilling, J. L. Brown, G. Goldhaber, S. Goldhaber, J. A. Kadyk, and J. Scanio, Phys. Letters 19, 427 (1965).

19. F. J. Gilman, Phys. Letters 29B, 673 (1969).

20. J. S. Loos, U. E. Kruse and E. L. Goldwasser, Phys. Rev. 173, 1330 (1968).

21. Birmingham-Glasgow-London(I.C.)-Oxford Rutherford Collaboration, Phys. Rev. 152, 1148 (1966).

22. Mott et al., Phys. Rev. 177, 1966 (1969). See also: J. Mott, Nucl. Phys. B13, 565 (1969).

23. L. Stodolsky and J. J. Sakurai, Phys. Rev. Letters 11, 90 (1963).

24. G. S. Abrams and B. H. Hall, private communication.

25. Joel Yellin, Phys. Rev. 147, 1080 (1966).

26. G. Alexander, H. Lipkin, and F. Scheck, Phys. Rev. Letters 17, 412 (1966).

27. Y. Pan and F. L. Forman, Phys. Rev. Letters 23, 806 (1969).

FIGURE CAPTIONS

Fig. 1. Most frequent strange particle topologies found in this experiment.

Fig. 2. Definition of the bubble chamber coordinate system. The y-axis is in the direction of the 72-inch chamber, i.e., approximately in the beam direction. The z-axis is approximately along the direction of the magnetic field and into the cameras. The origin is placed approximately at the bottom of the chamber, midway between the entrance and exit ends, and midway between the sides of the chamber. The angle φ is called the azimuthal angle. The angle λ is called the dip angle.

Fig. 3. Scatter plot of the center-of-mass decay cosine versus the lab decay azimuth for the $\Sigma^+ \rightarrow n\pi^+$ decay. The plot contains 753 Σ^+ decays.

Fig. 4. (a) For 176 events ambiguous between reactions iv and v of Table I, the distribution of decay cosine of the photon w. r. t. the beam direction, both directions taken in the Σ^o center of mass. (b) Same, except w. r. t. the outgoing π^+. (c) Same, except w. r. t. the K^+. (d) Scatter plot of the cosine from Fig. 4b versus the cosine from Fig. 4c for these events where the events in the peak of Fig. 4a have been removed. 75 events. (e) Same distribution as Fig. 4a for events which fit reaction v unambiguously.

Fig. 5. Dalitz plot for reaction ii of Table I for 48 events where the K^o is visible.

Fig. 6. Distribution of π^+K^o mass for reaction ii.

Fig. 7. Dalitz plot for reaction iv of Table I for 239 events where the Λ is visible.

Fig. 8. Distribution of $\Lambda\pi^+$ mass for reaction iv.

Fig. 9. Dalitz plot for reaction vi of Table I for 92 events where the K^o is visible.

Fig. 10. Distribution of $K^+\overline{K^o}$ mass for reaction iv.

Fig. 11. Triangle plot for reaction vii of Table I for 323 unambiguous events.

Fig. 12. Distribution of $p\pi^+$ mass for reaction vii.

Fig. 13. Distribution of K^+K^- mass for reaction vii.

Fig. 14. Distribution of K^+K^- mass for reaction vii for 161 events with $p\pi^+$ mass between 1160 MeV and 1280 MeV.

Fig. 15. Distribution of π^+K^- mass for reaction vii.

Fig. 16. Distribution of pK^- mass for reaction vii.

Fig. 17. Distribution of $p\pi^+$ mass for reaction vii for the 27 events with K^+K^- mass in the φ band.

Fig. 18. Distribution of $p\pi^+$ mass for $p\pi^+K^o\overline{K^o}$, (a) 39 events with two visible vees, corresponding to $p\pi^+K_1^oK_1^o$, (b) 110 events with one visible vee, (c) appropriate subtraction to give distribution corresponding to $p\pi^+K_1^oK_2^o$.

Fig. 19. Distribution of π^+K^o mass for $p\pi^+K^o\overline{K^o}$, each event plotted twice. (a), (b) and (c) as for Fig. 18.

Fig. 20. Distribution of $K^o\overline{K^o}$ mass for $p\pi^+K^o\overline{K^o}$, (a), (b) and (c) as for Fig. 18.

Fig. 21. Distribution of pK^o mass for $p\pi^+K^o\overline{K^o}$, each event plotted twice. (a), (b) and (c) as for Fig. 18.

Fig. 22. Distribution of momentum transfer, t, for reaction i of Table I. (a) Region of the fit, resulting slope is (8.4 ± 1.4) $(GeV/c)^{-2}$.

(b) Entire distribution where the first 6 points have been replaced by the fitted curve. The maximum -t of 5.6 $(GeV/c)^2$ corresponds to an incident momentum of 3.8 GeV/c. The point between 2 and 4 $(GeV/c)^2$ is determined by only one event.

Fig. 23. Distribution of $t' = |t| - |t|_{min}$ for $\pi^+ p \rightarrow \Sigma(1385)^+ K^+$. The fit, taken over the four interior points, gives a slope of (3.0 ± 0.6) $(GeV/c)^{-2}$.

Fig. 24. Decay distributions for the $\Sigma(1385)^+$ in the Jackson frame. (a) is $\cos(\alpha)$ and (b) is the azimuthal angle φ. The curves are predicted from the model of Stodolsky and Sakurai.

Fig. 25. Distribution of $\cos(\alpha)$ for the K^+K^- system for $\pi^+ p \rightarrow \Delta^{++} K^+ K^-$.

Fig. 26. Distribution of $\cos(\alpha)$ for the K^+K^- system for reaction vii of Table I, where the Δ^{++} has been removed.

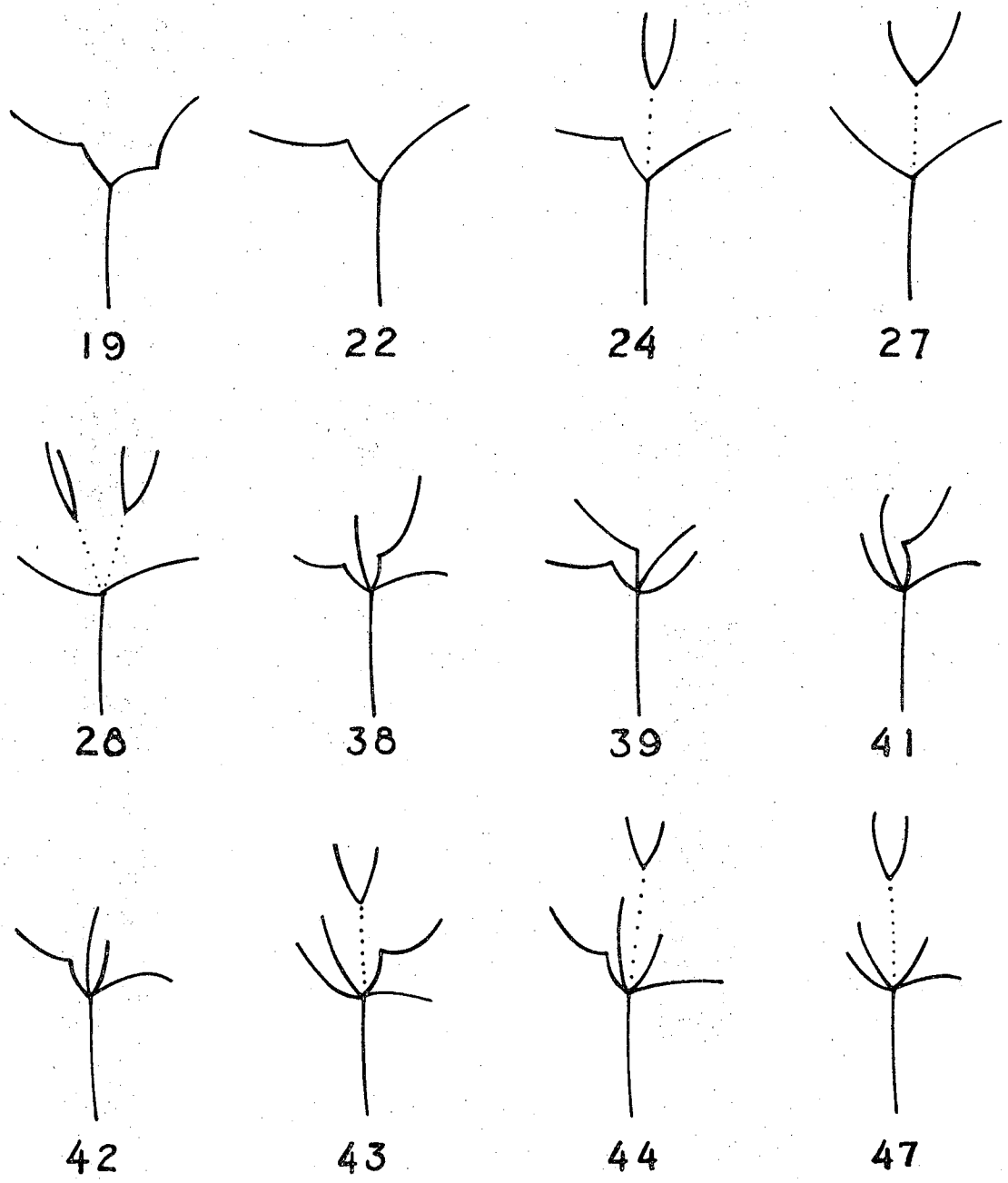

XBL 706-1117

Fig. 1

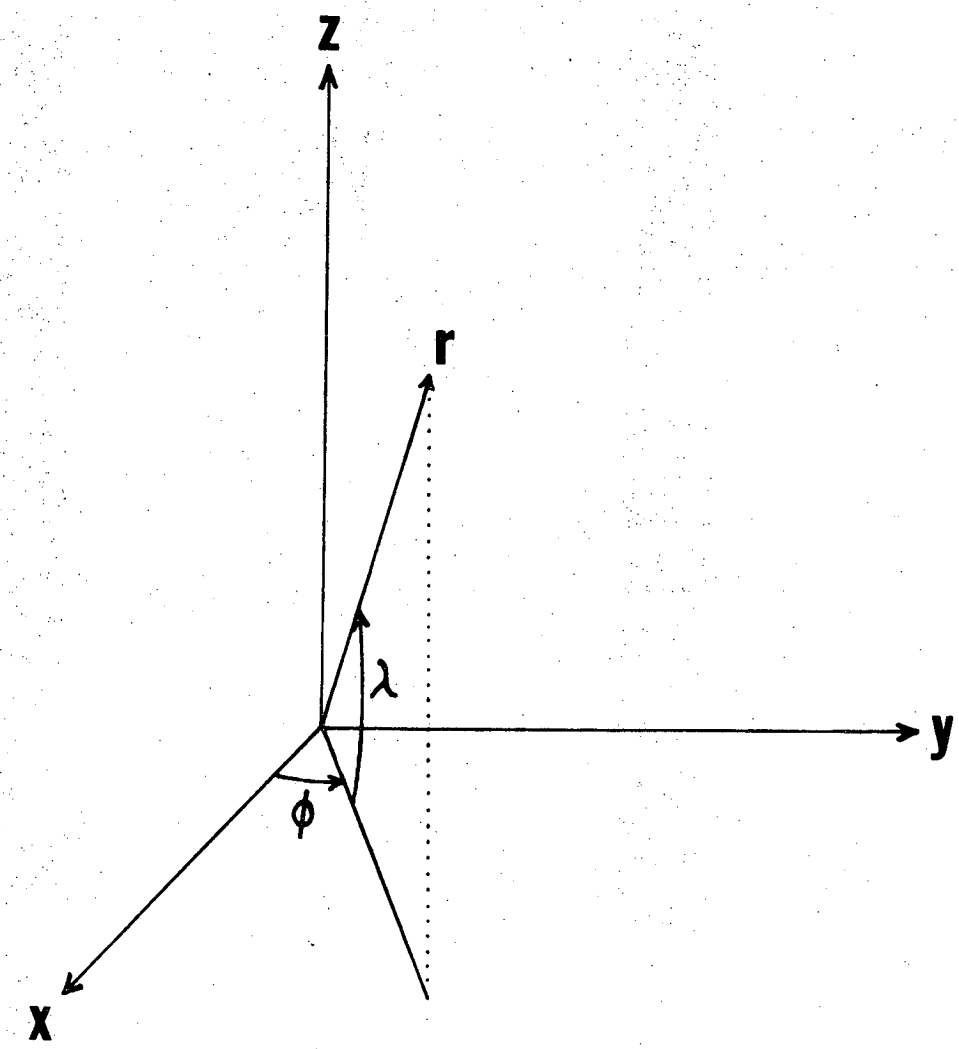

XBL 706-1118

Fig. 2

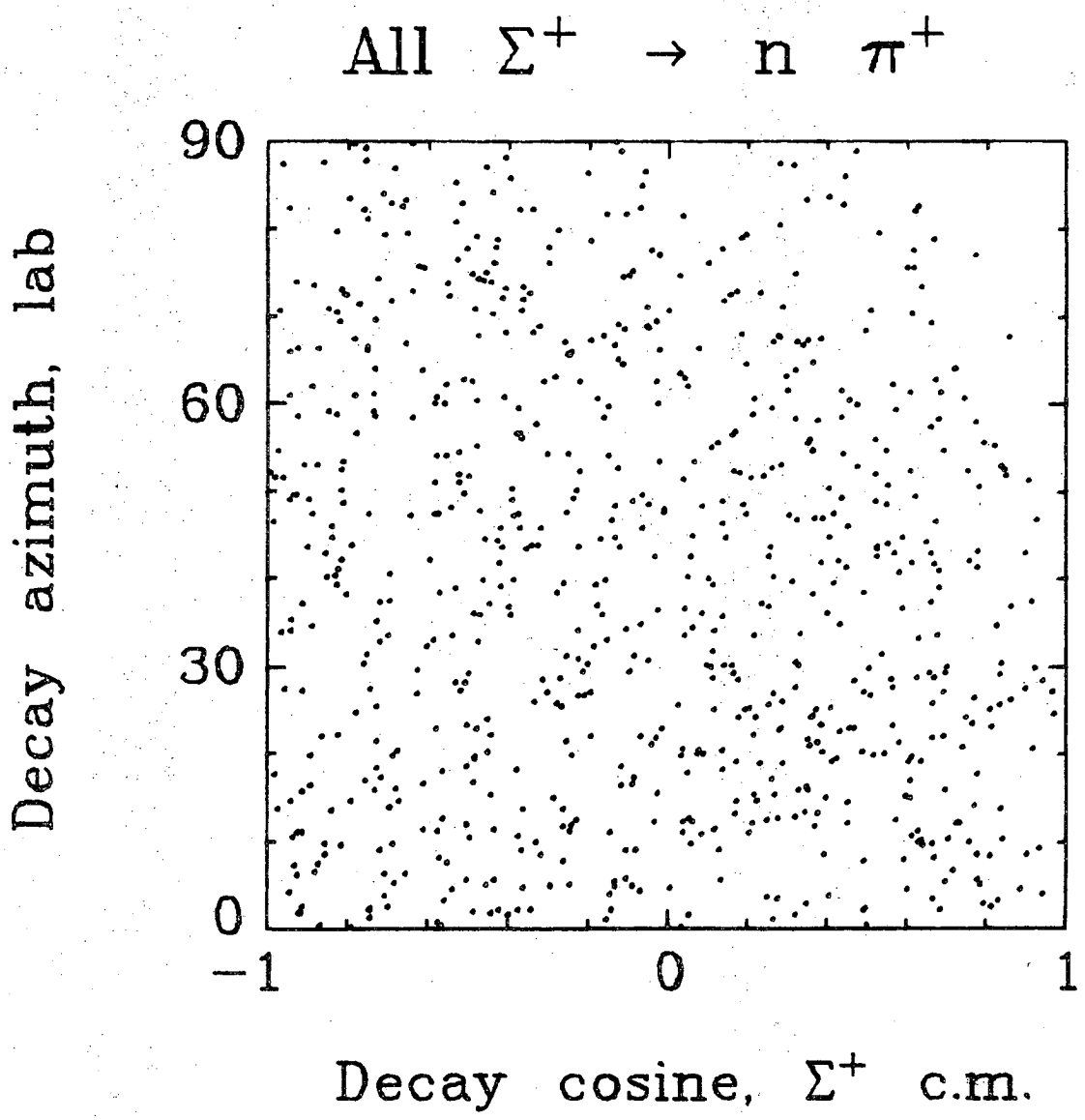

XBL 706-1140

Fig. 3

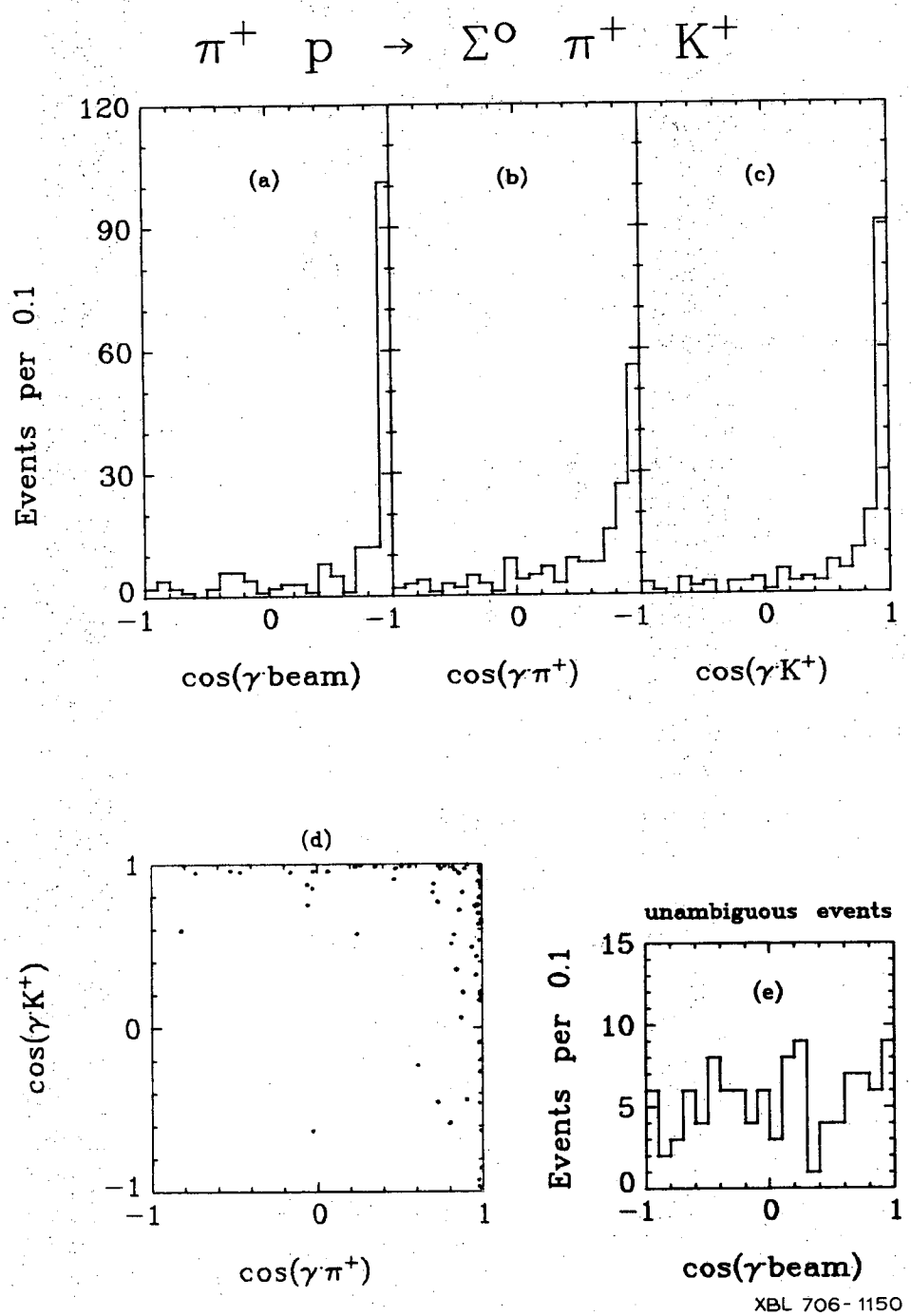
$\pi^+ \; p \rightarrow \Sigma^o \; \pi^+ \; K^+$
(a)
(b)
(c)
Events per 0.1
120
90
60
30
0
−1
0
1
cos(γ·beam)
cos(γ·π+)
cos(γ·K+)
(d)
cos(γ·K+)
cos(γ·π+)
unambiguous events
(e)
Events per 0.1
15
10
5
cos(γ·beam)
XBL 706-1150

Fig. 4

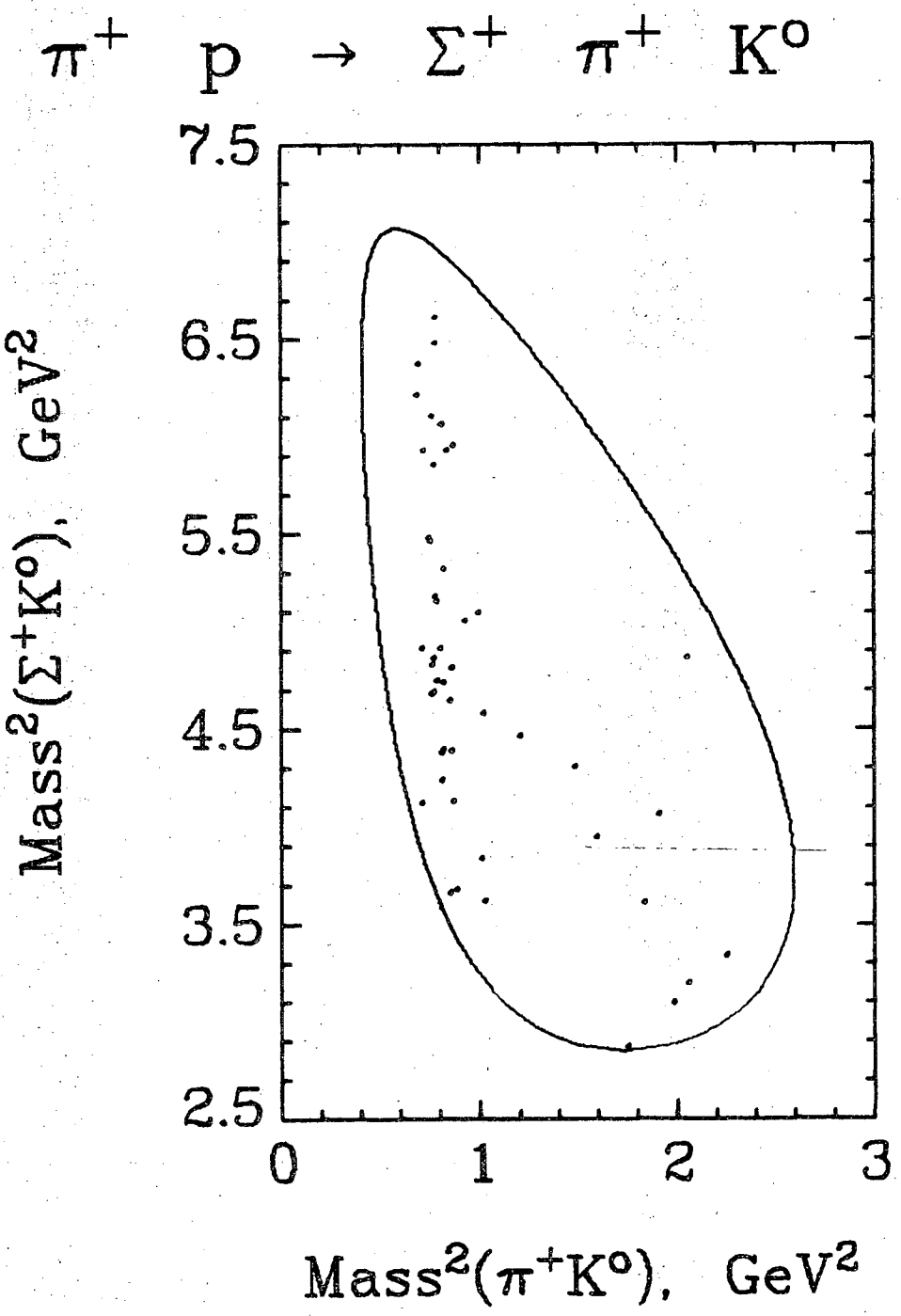

XBL 706-1145

Fig. 5

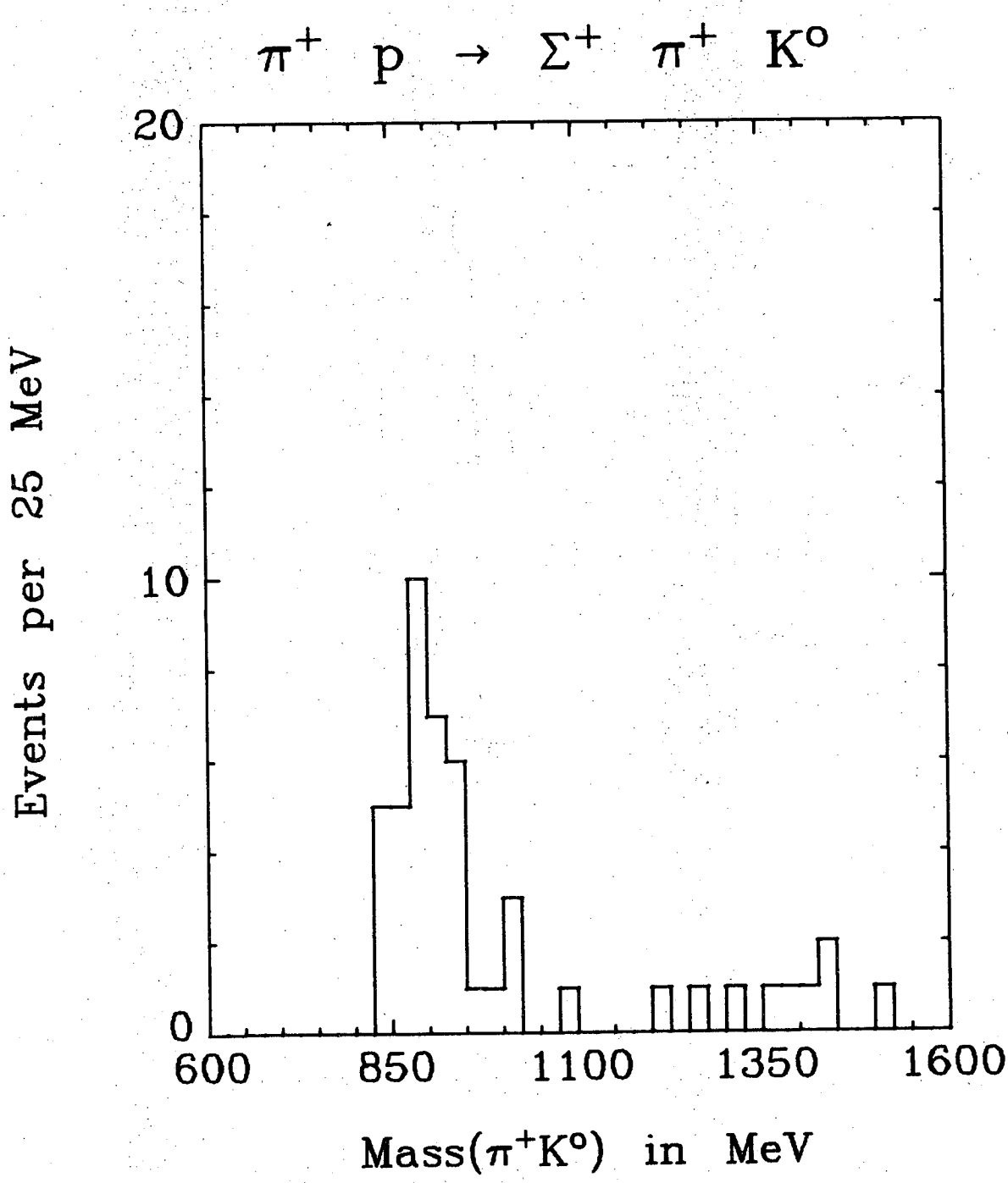

XBL 706-1144

Fig. 6

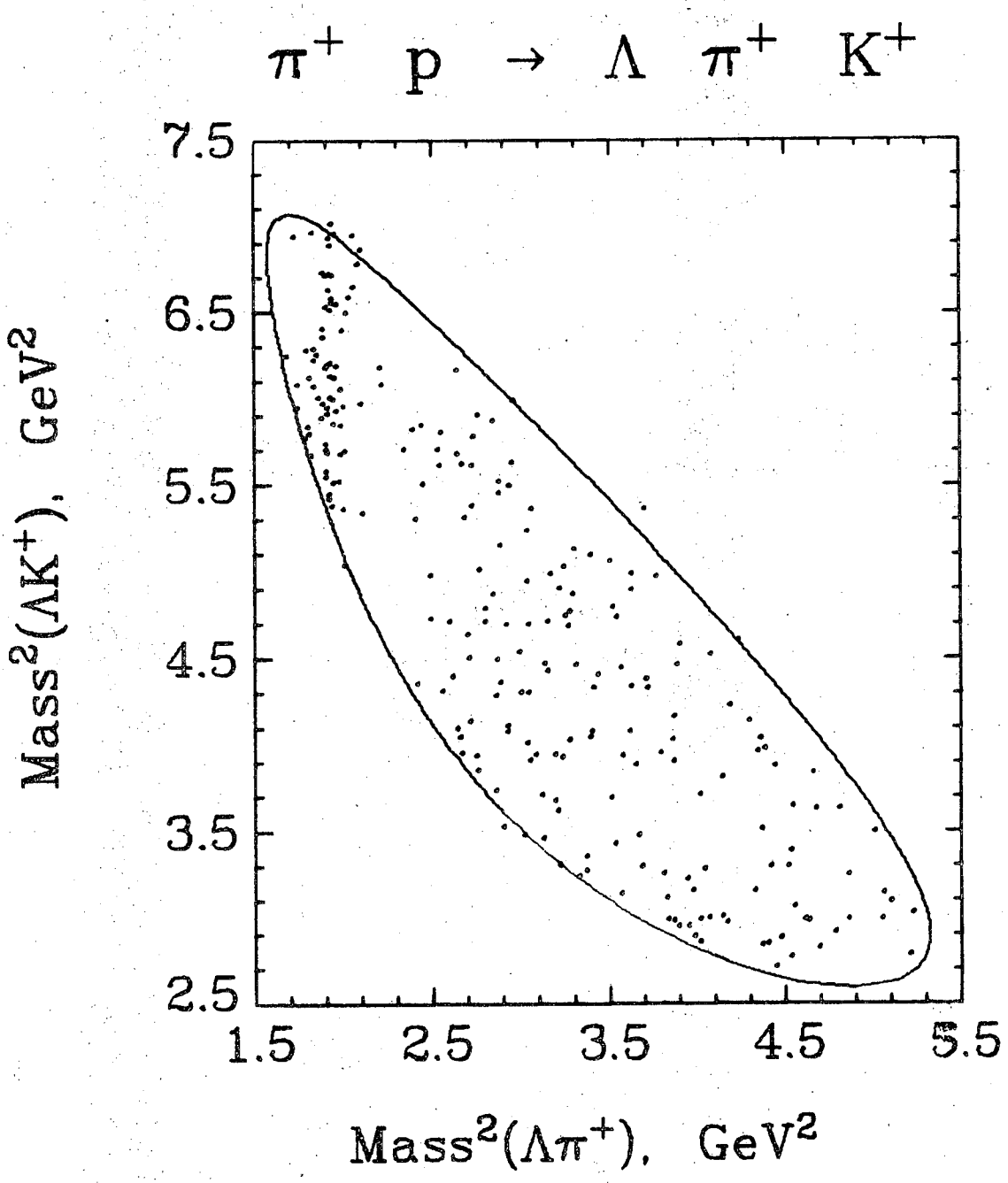

XBL 706-1143

Fig. 7

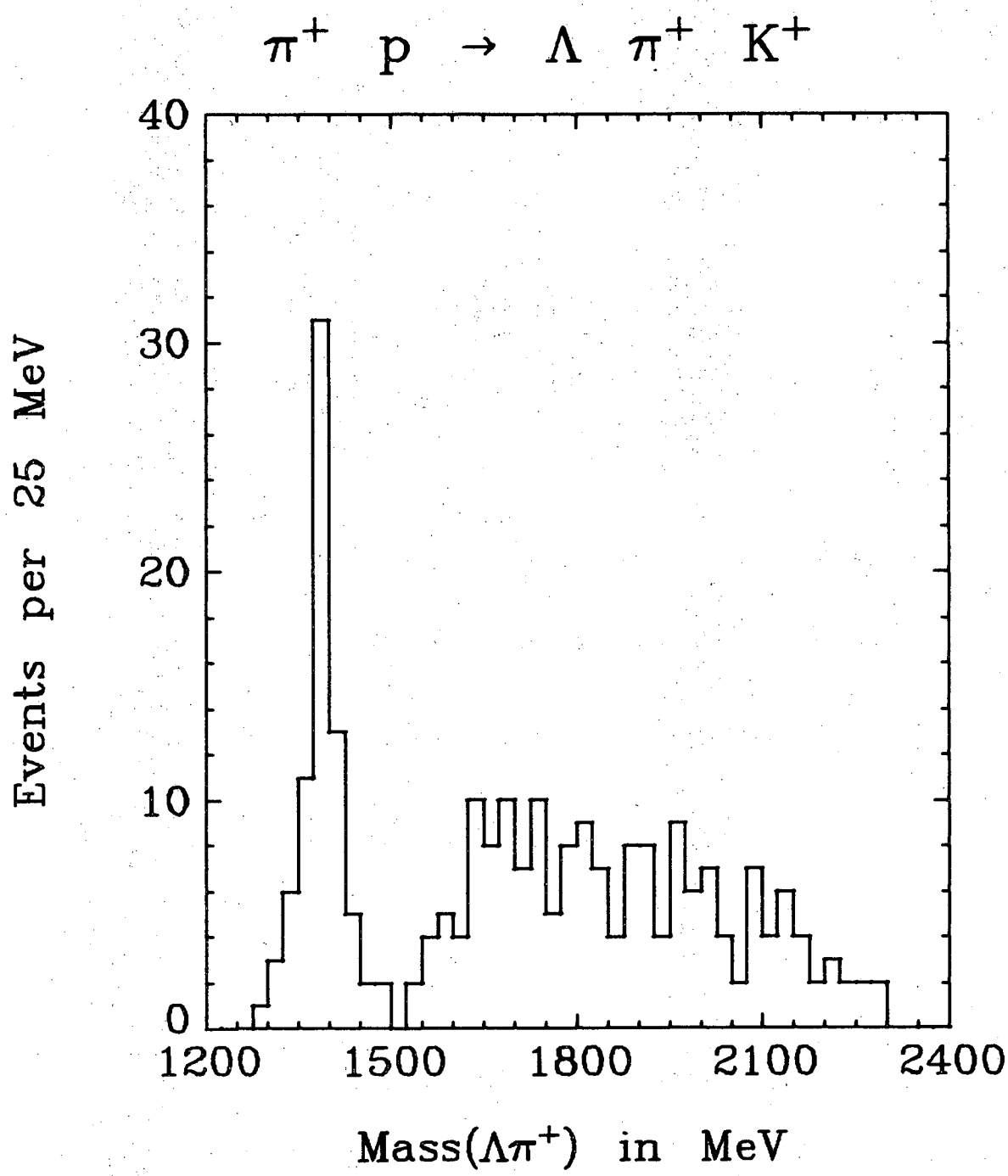

XBL 706-1142

Fig. 8

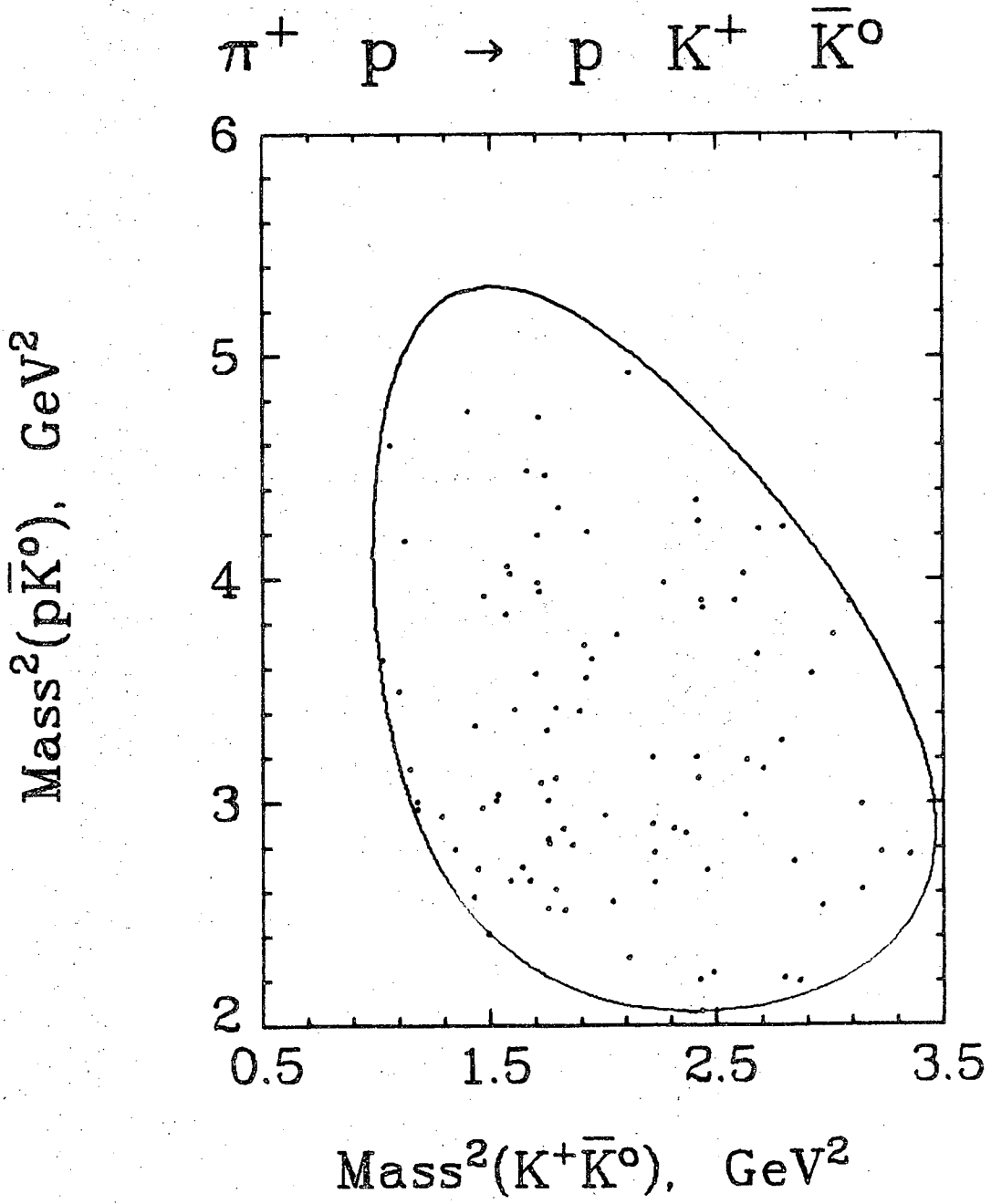

XBL 706-1141

Fig. 9

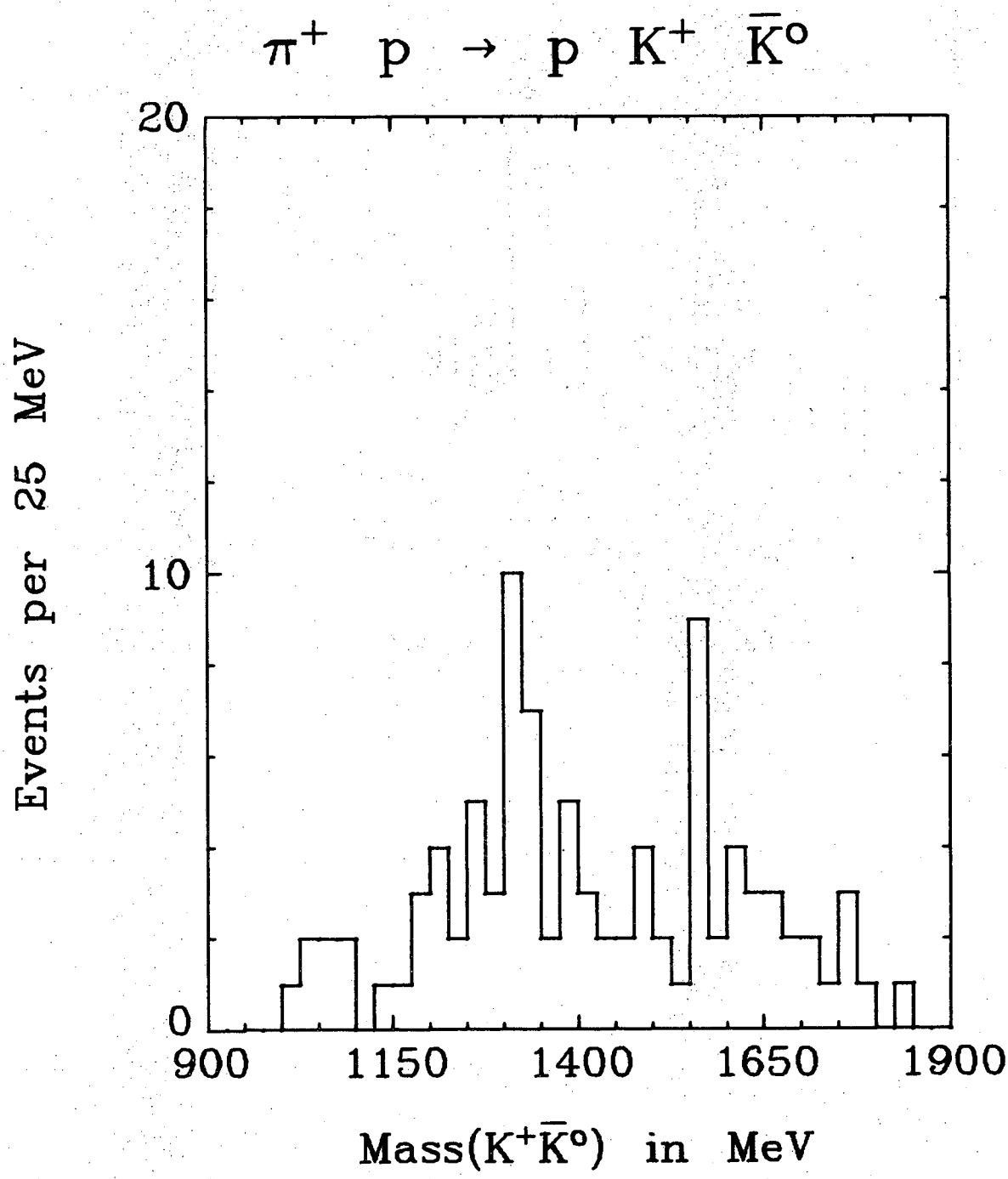

XBL 706-1148

Fig. 10

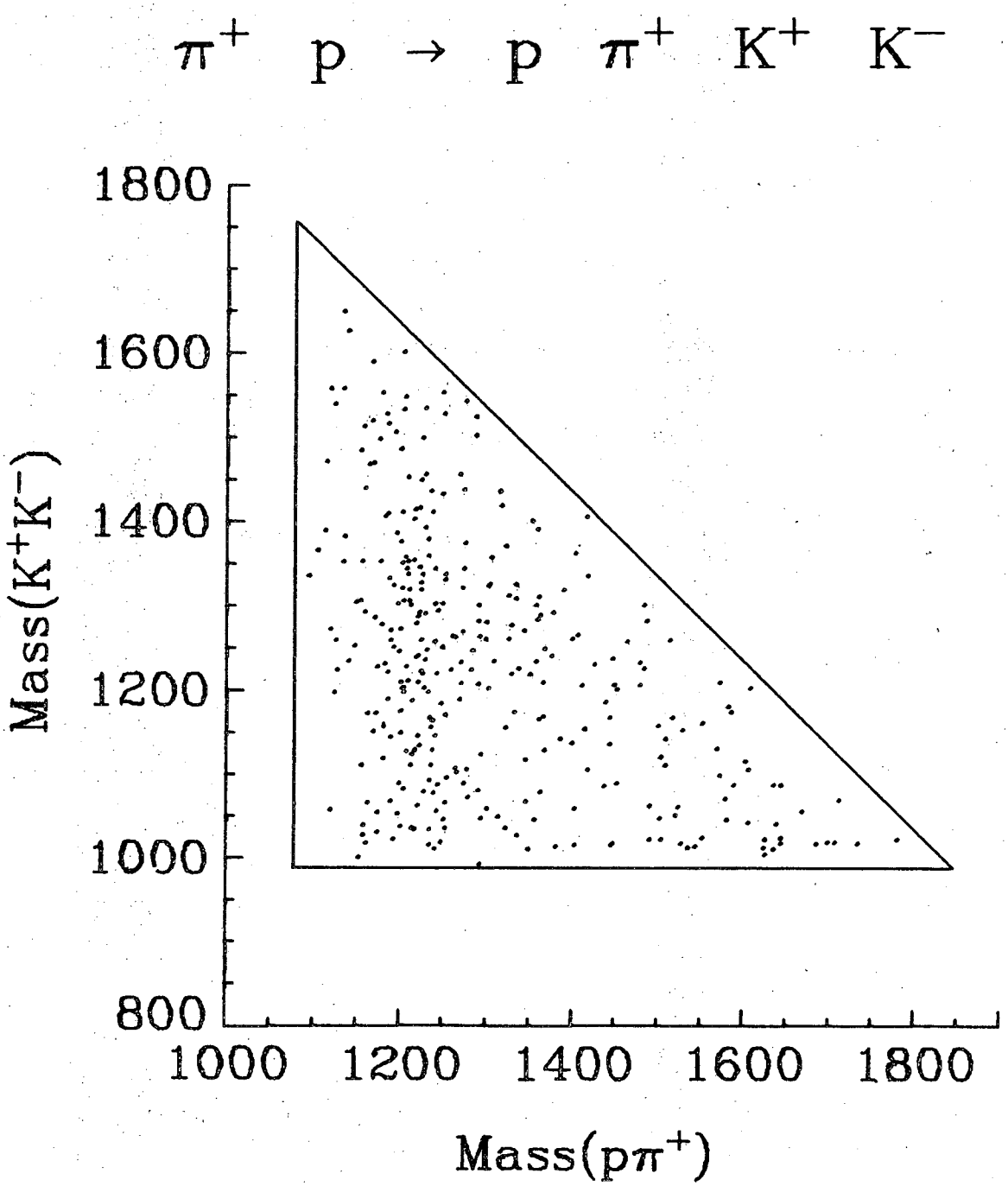

XBL 706-1139

Fig. 11

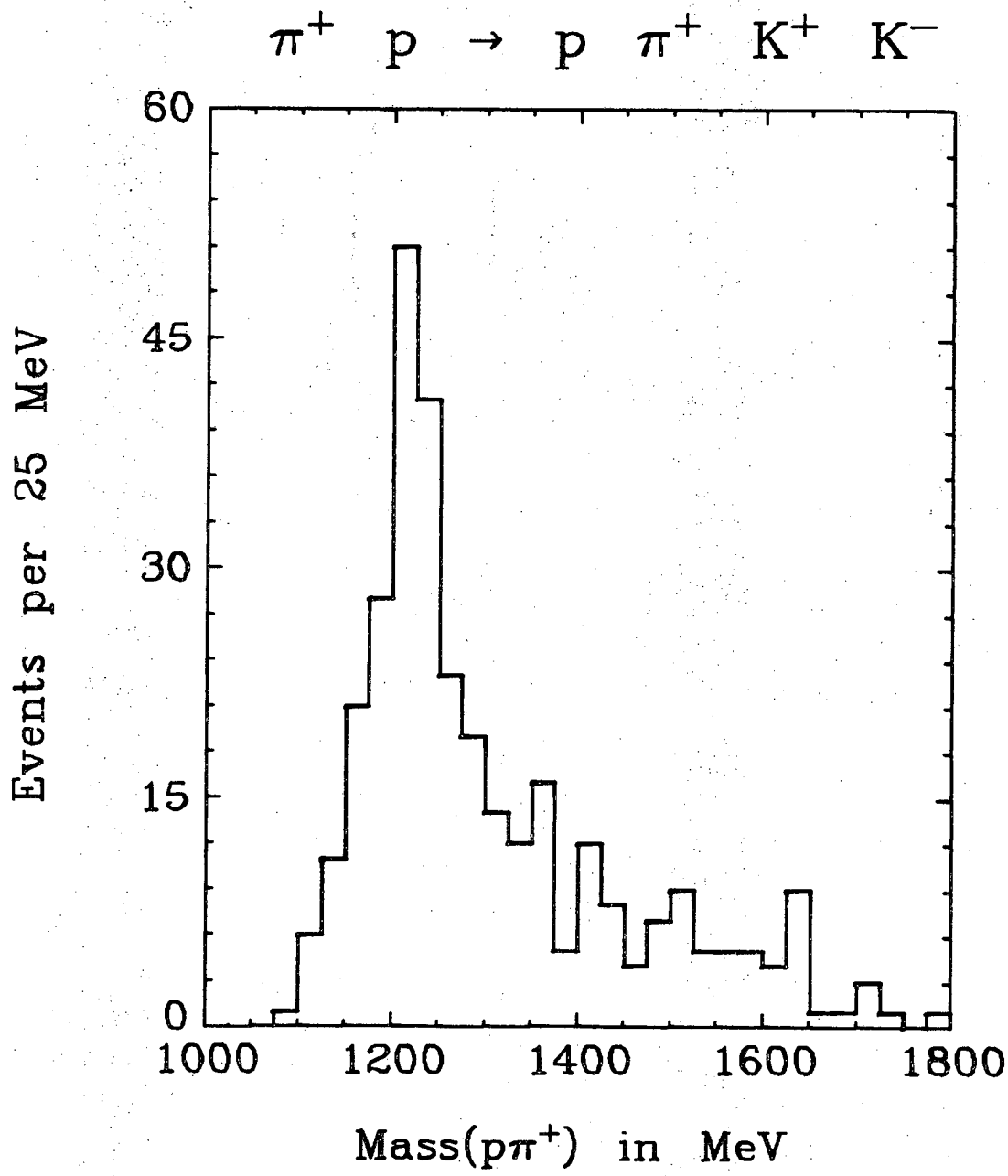

XBL 706-1119

Fig. 12

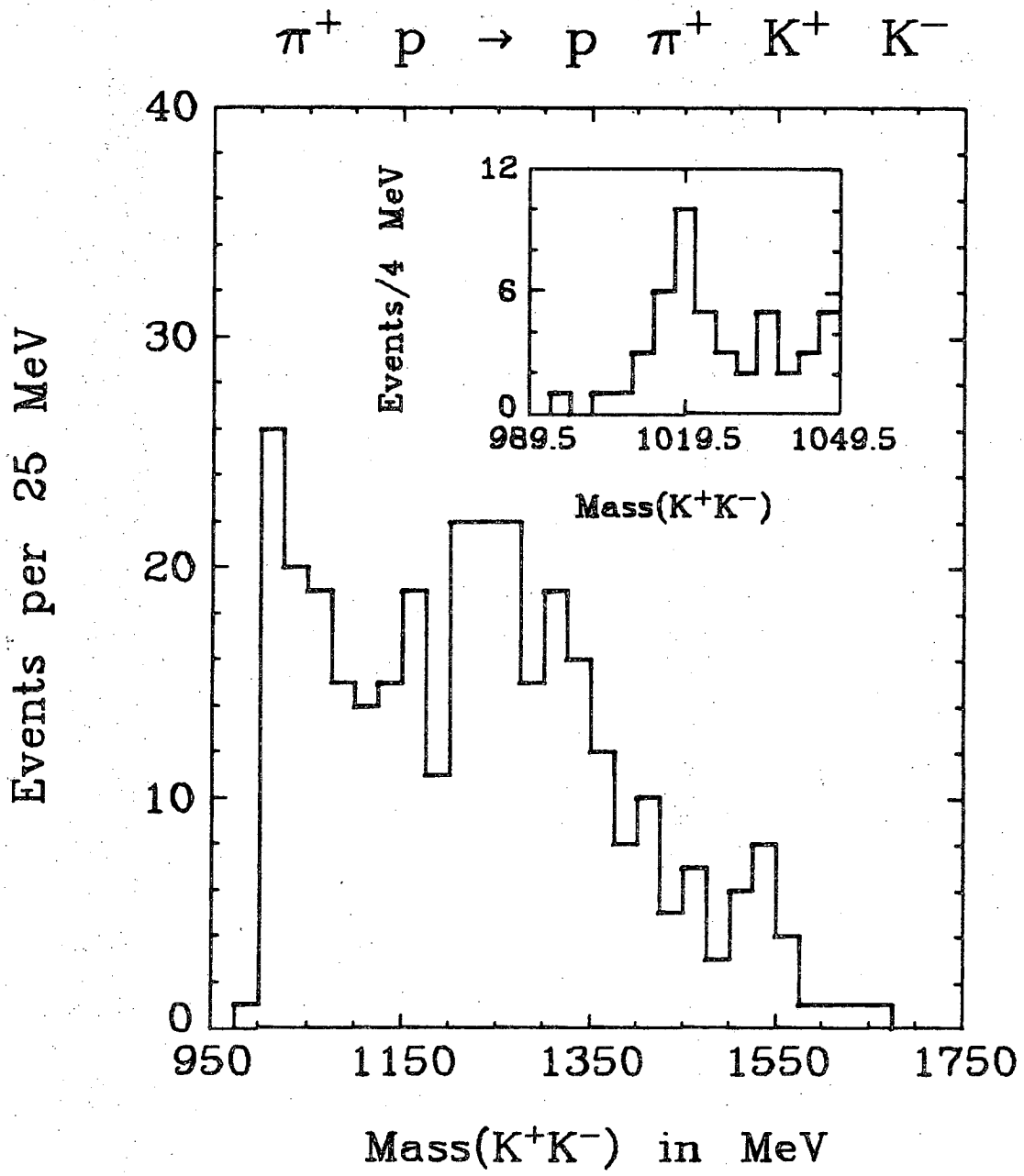

XBL 706-1120

Fig. 13

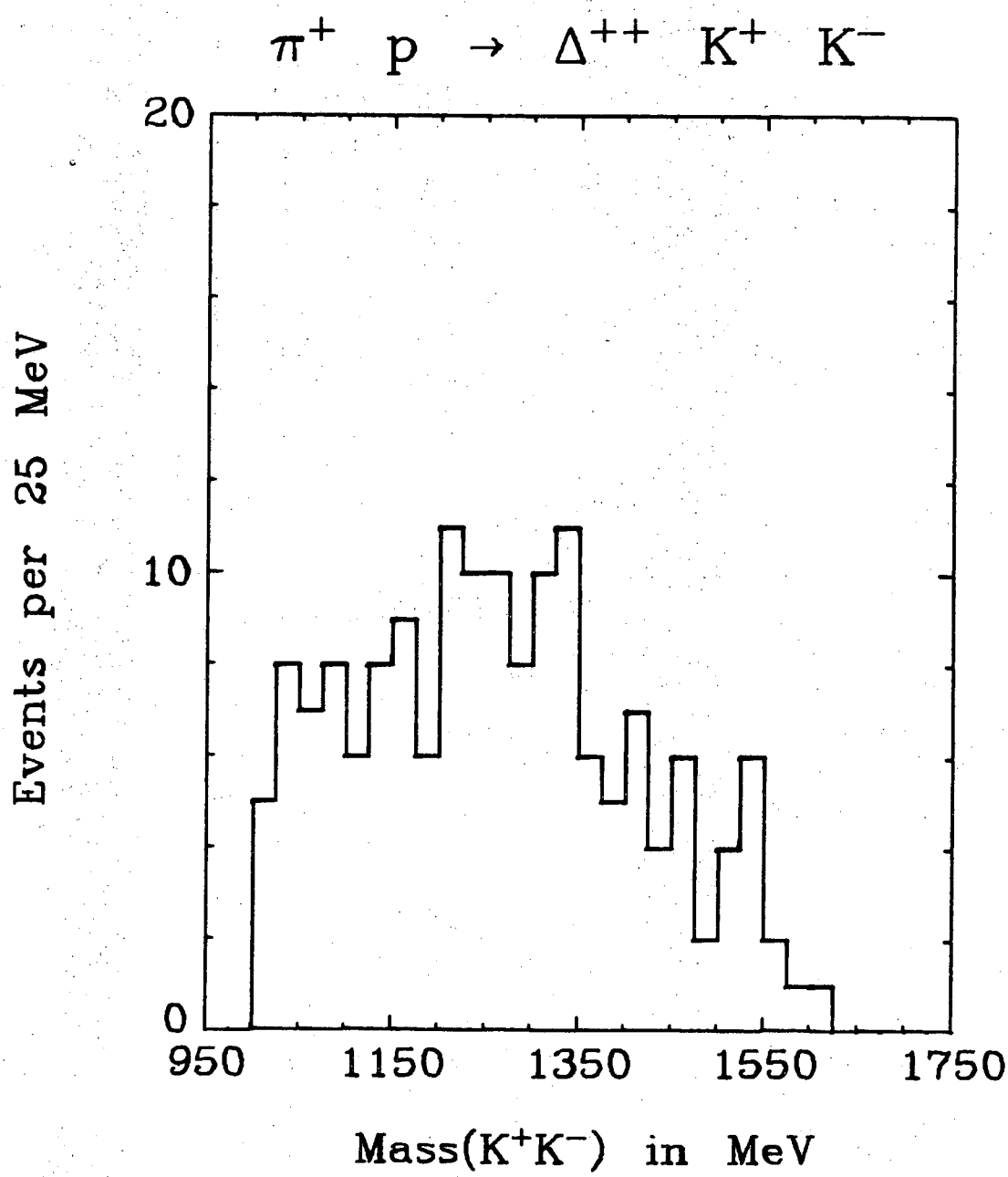

XBL 706-1121

Fig. 14

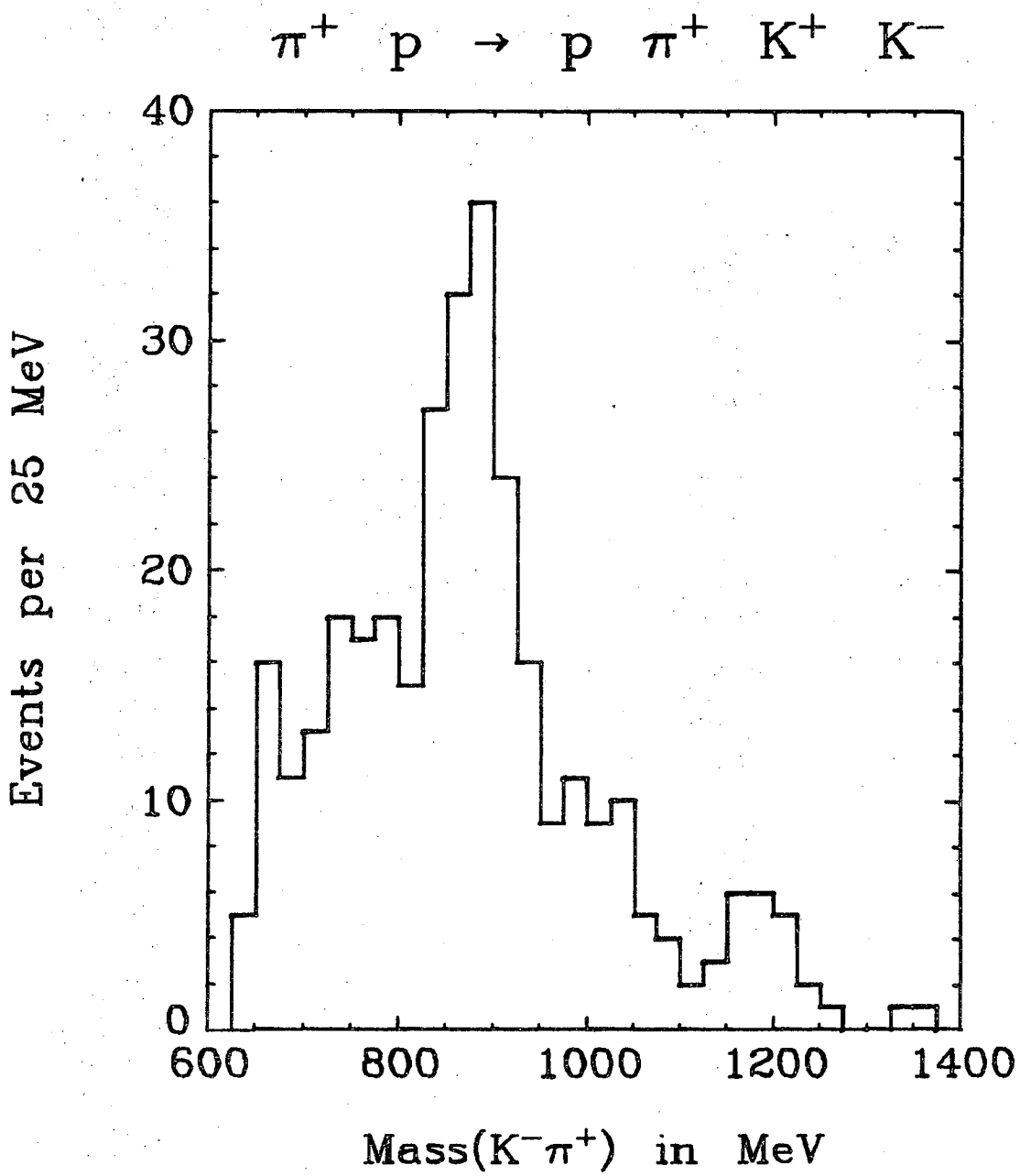

XBL 706-1122

Fig. 15

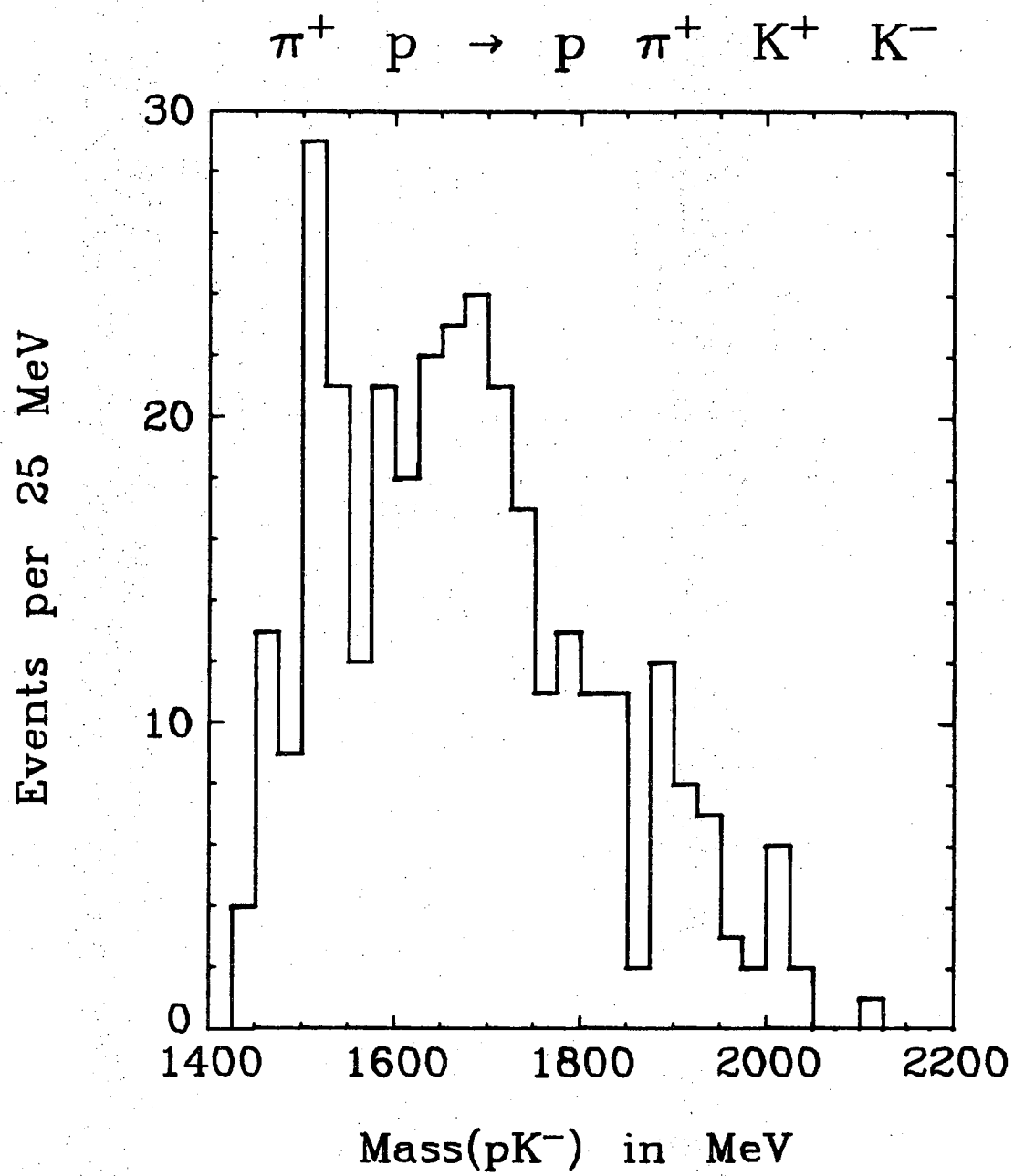

XBL 706-1123

Fig. 16

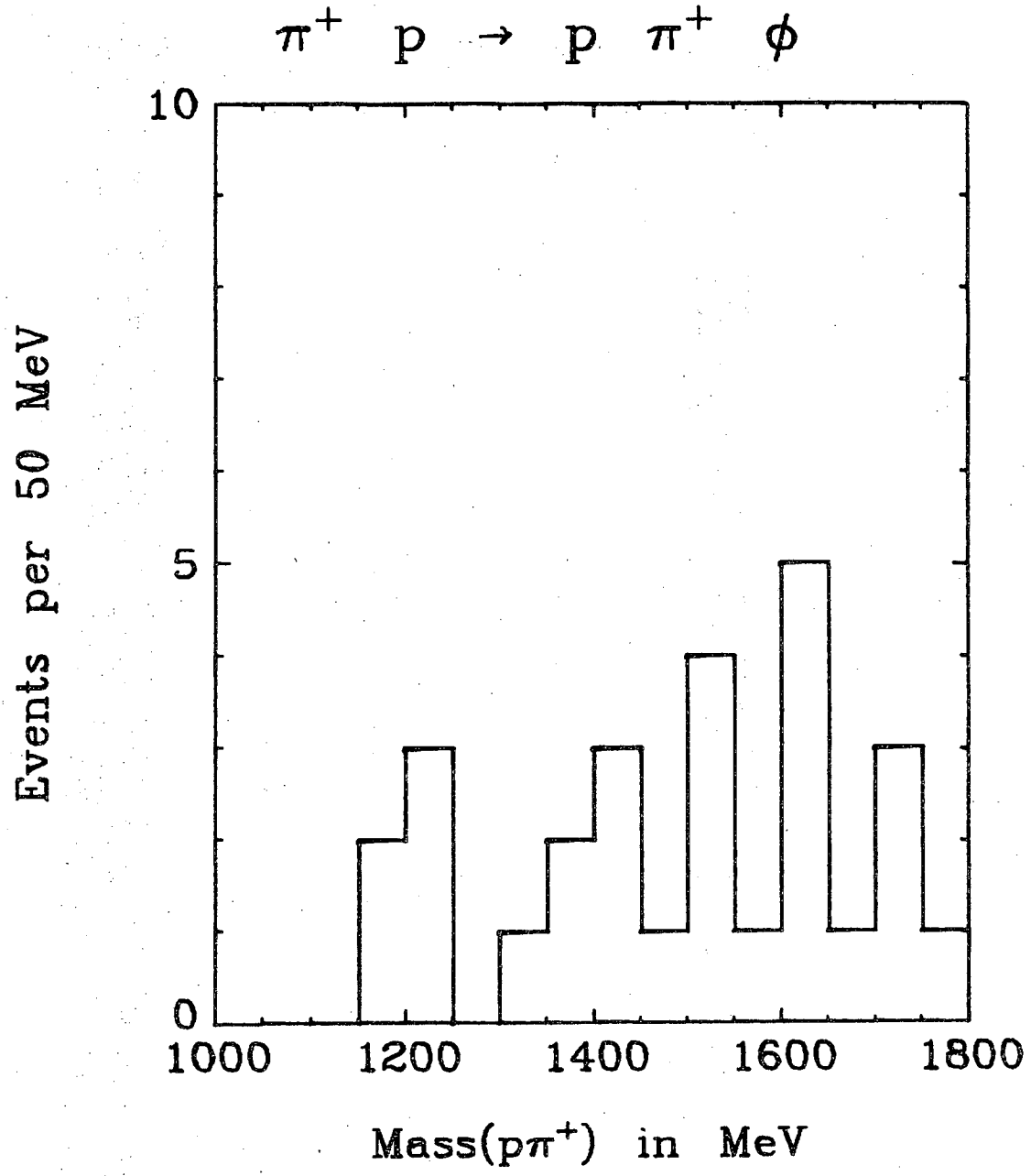

XBL 706-1124

Fig. 17

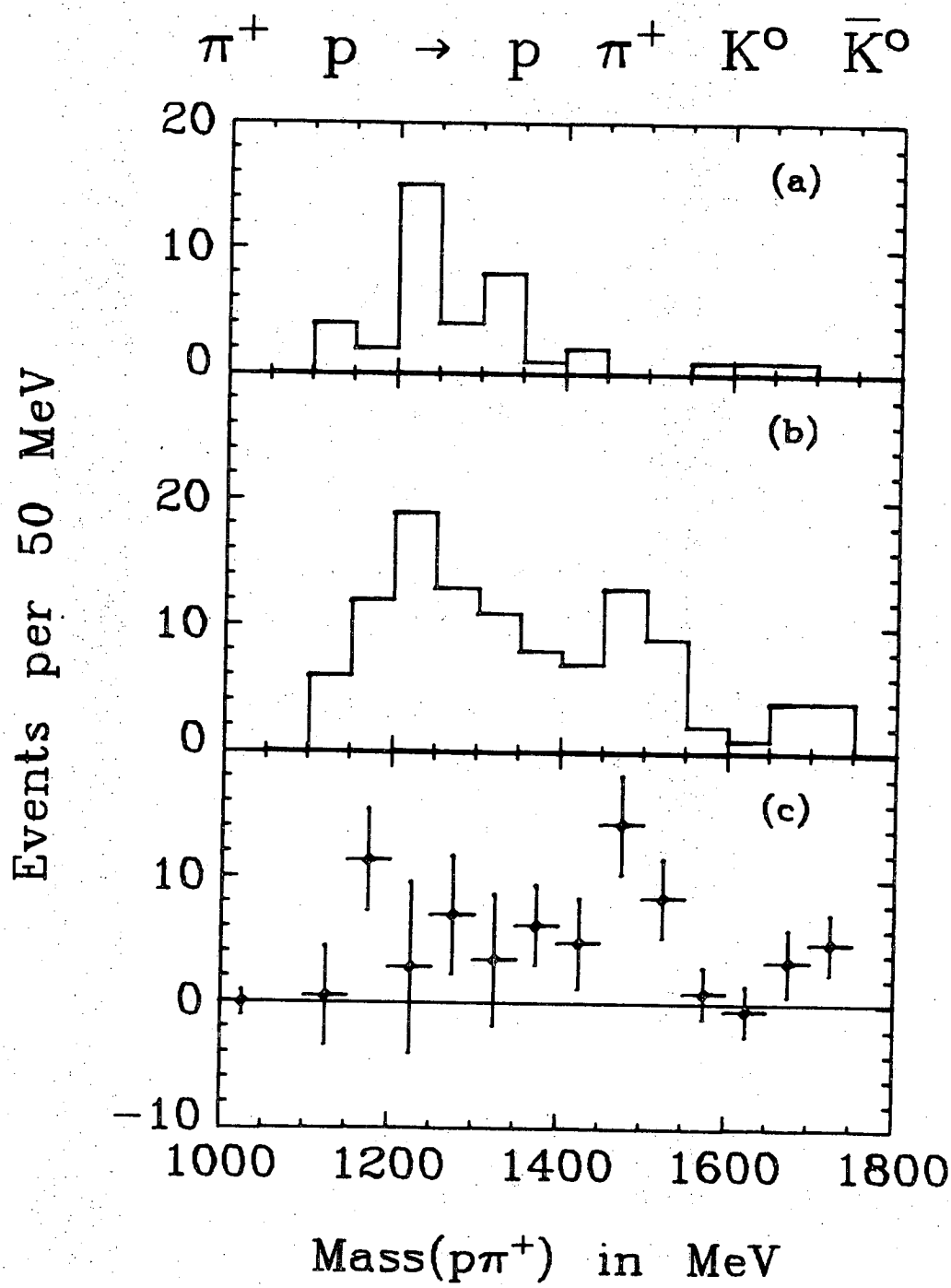

XBL 706-1126

Fig. 18

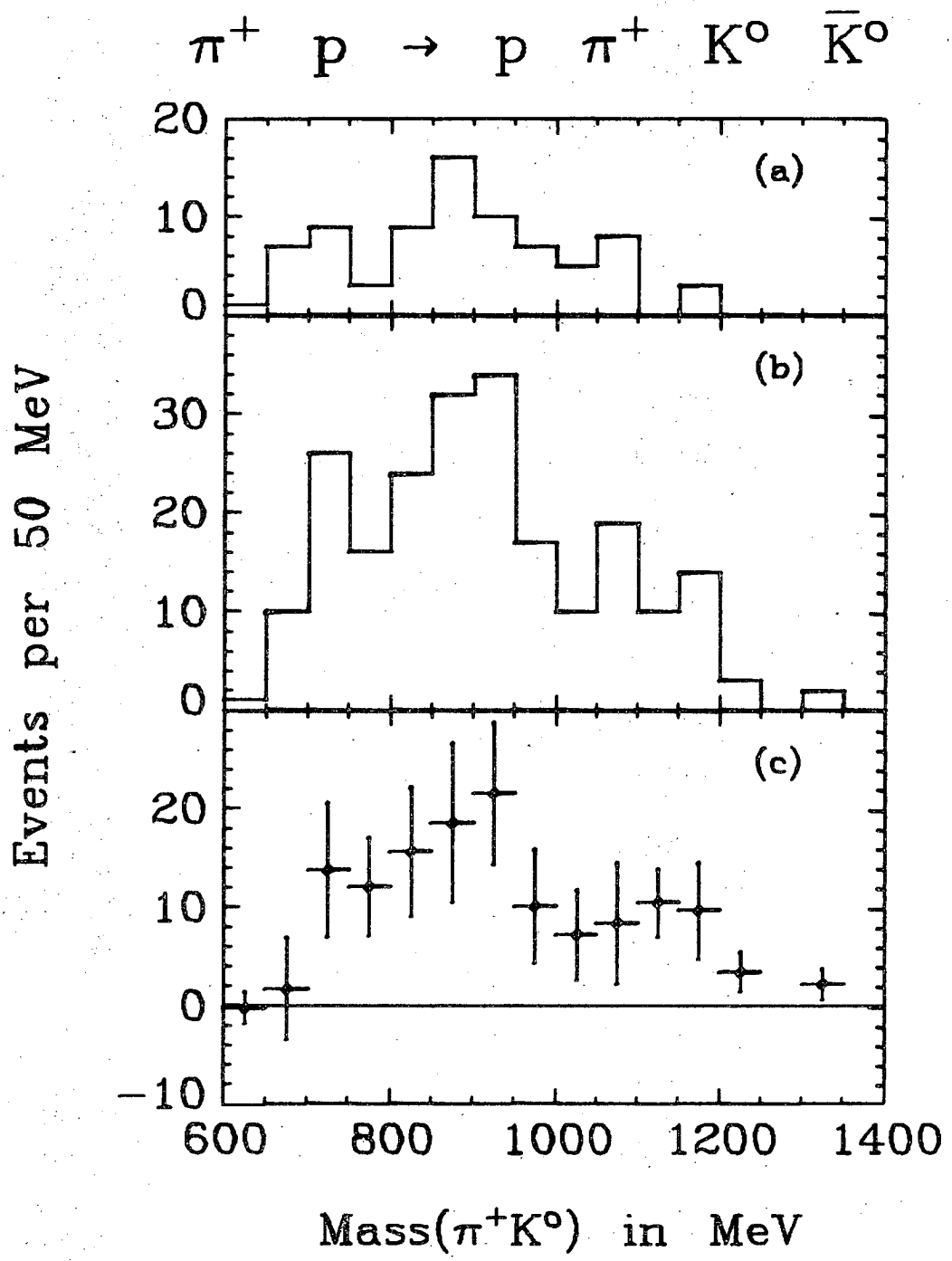

XBL 706-1128

Fig. 19

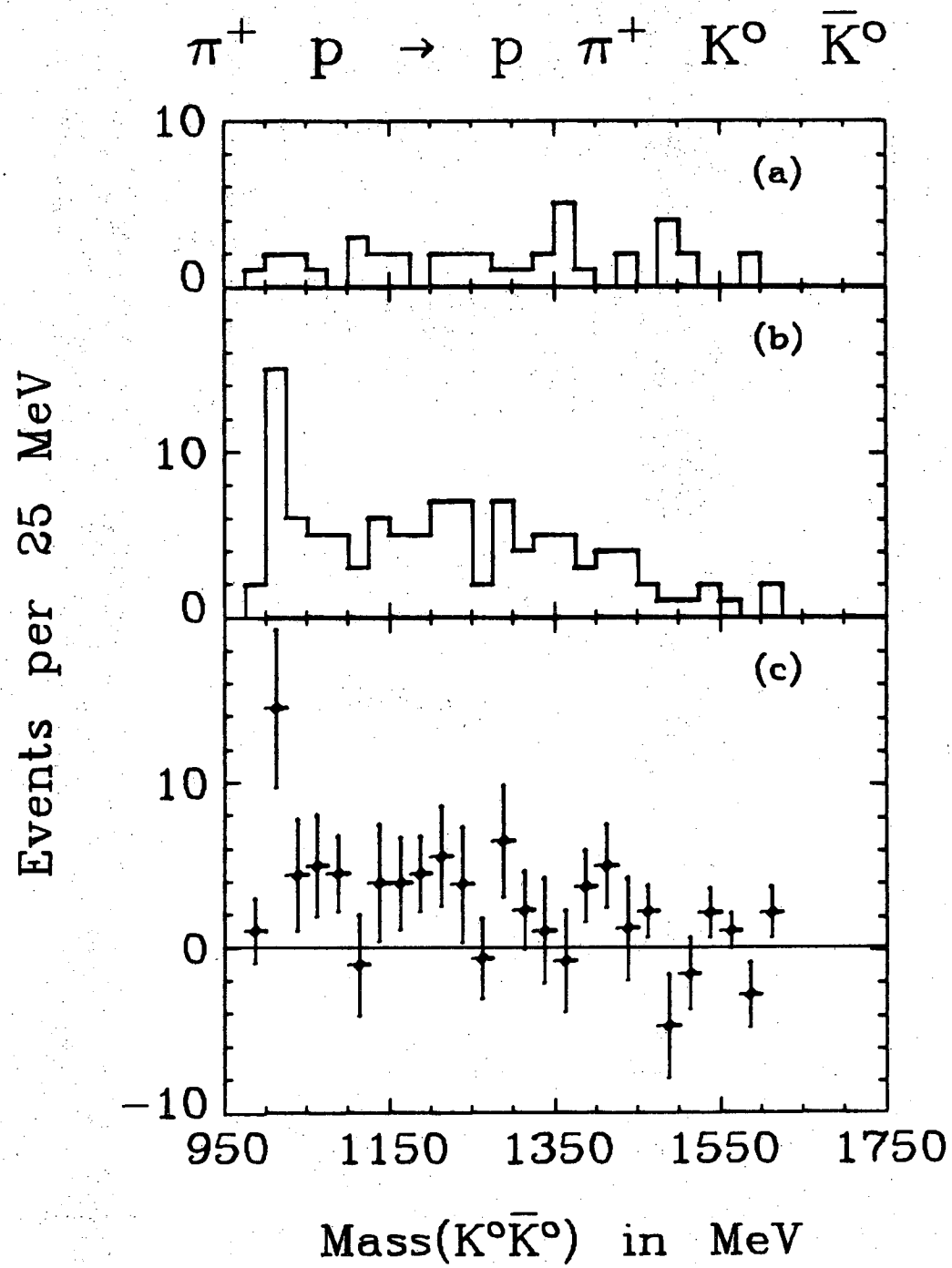

XBL 706-1129

Fig. 20

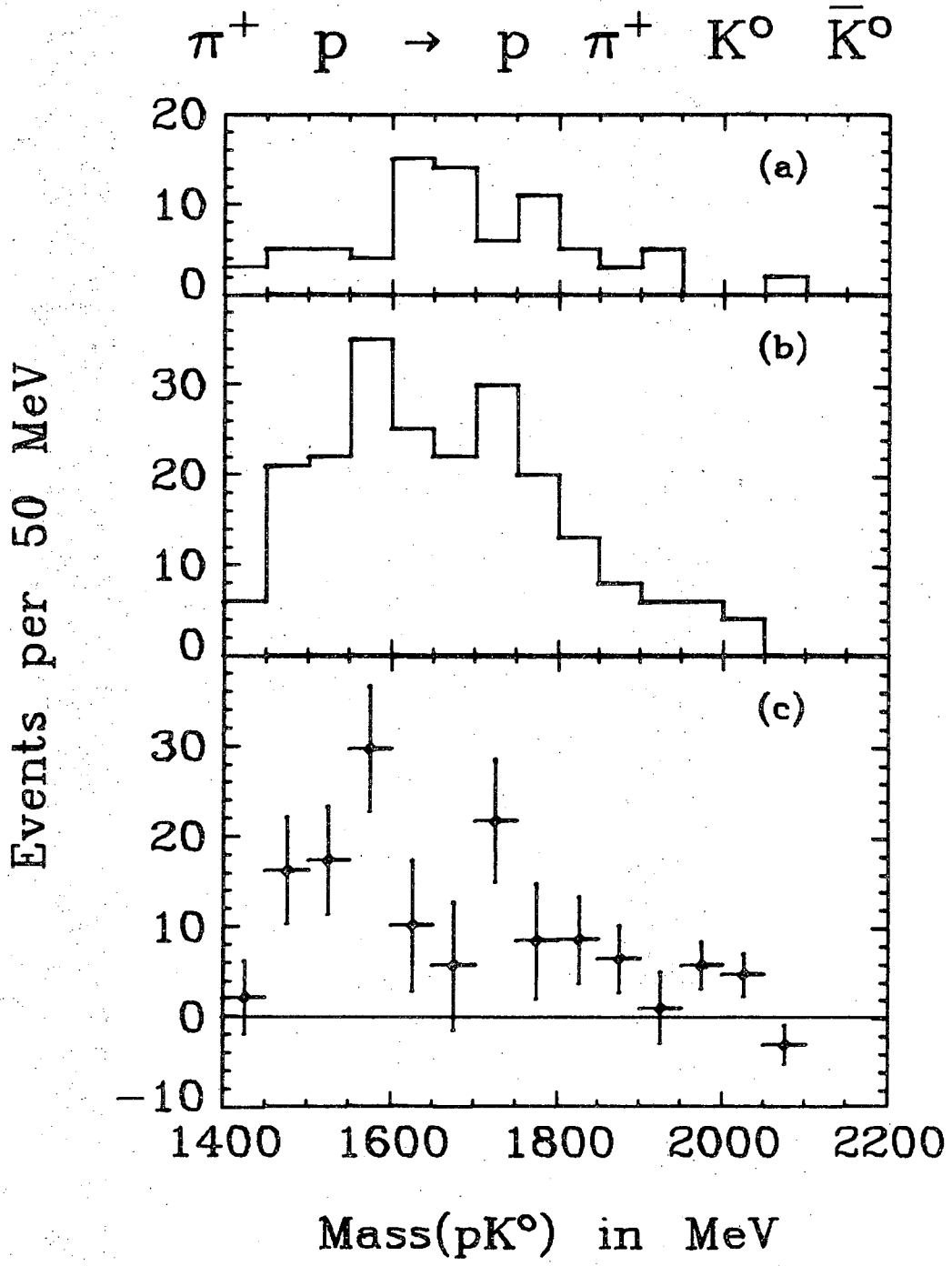

XBL 706-1127

Fig. 21

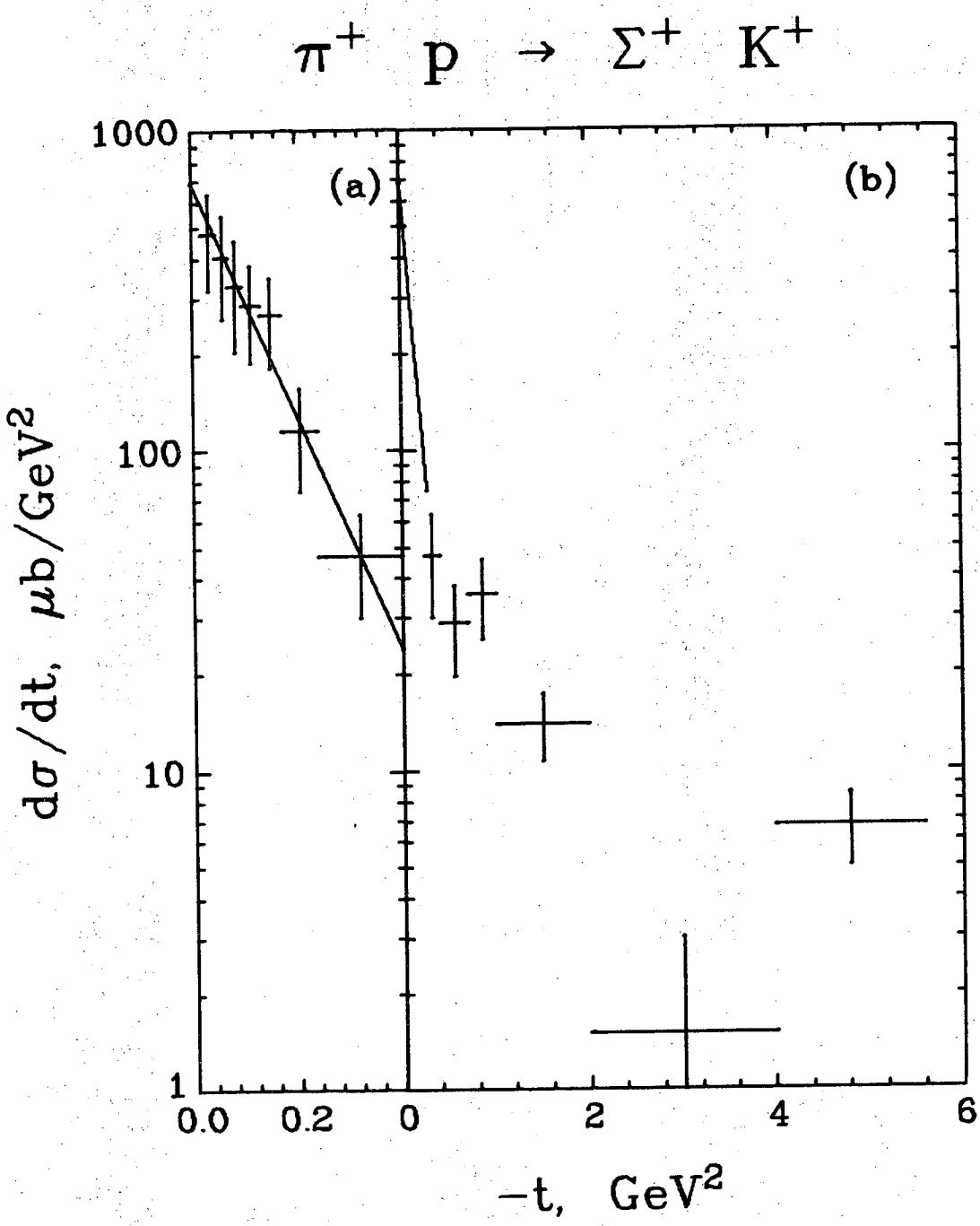

XBL 706-1149

Fig. 22

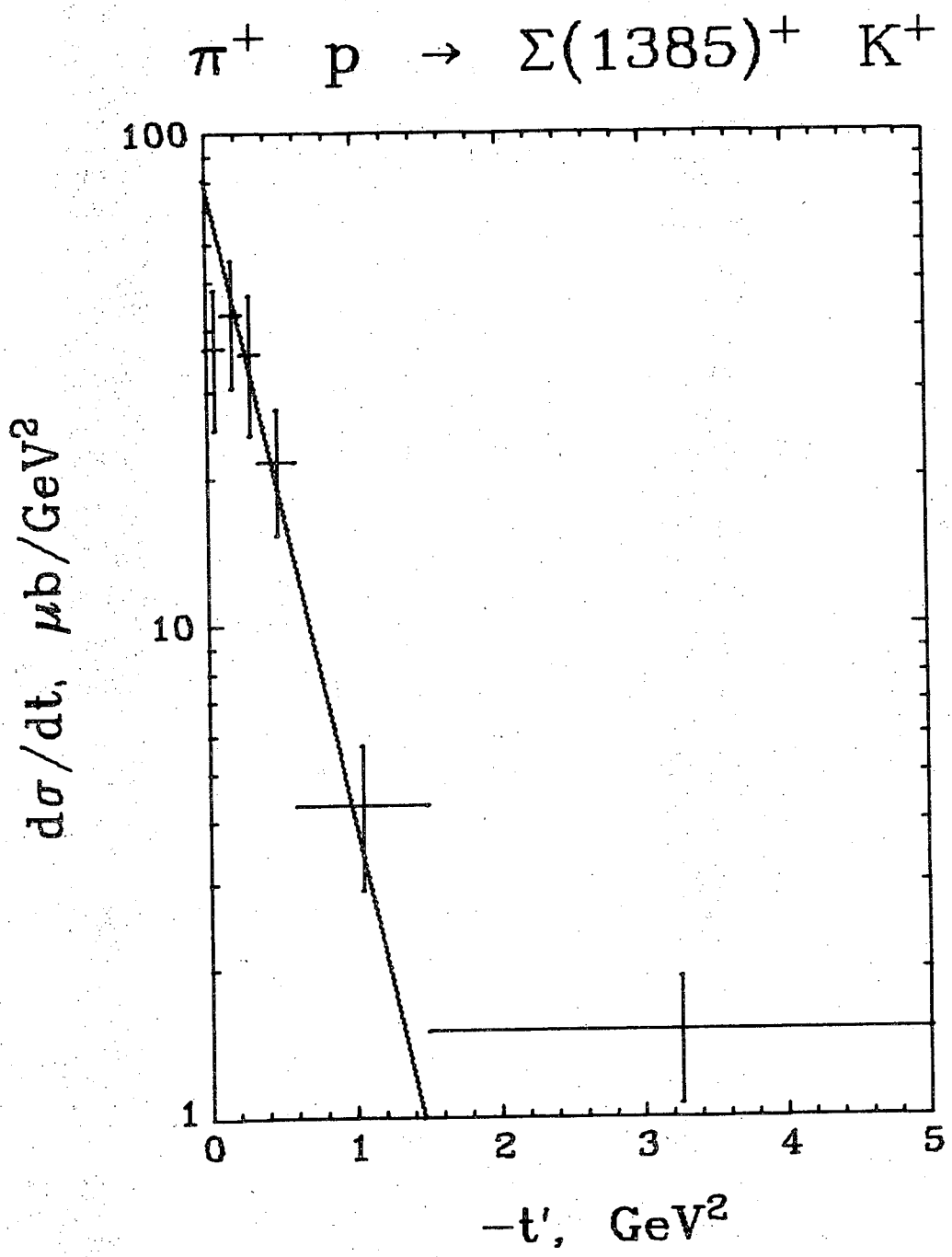

XBL 706-1147

Fig. 23

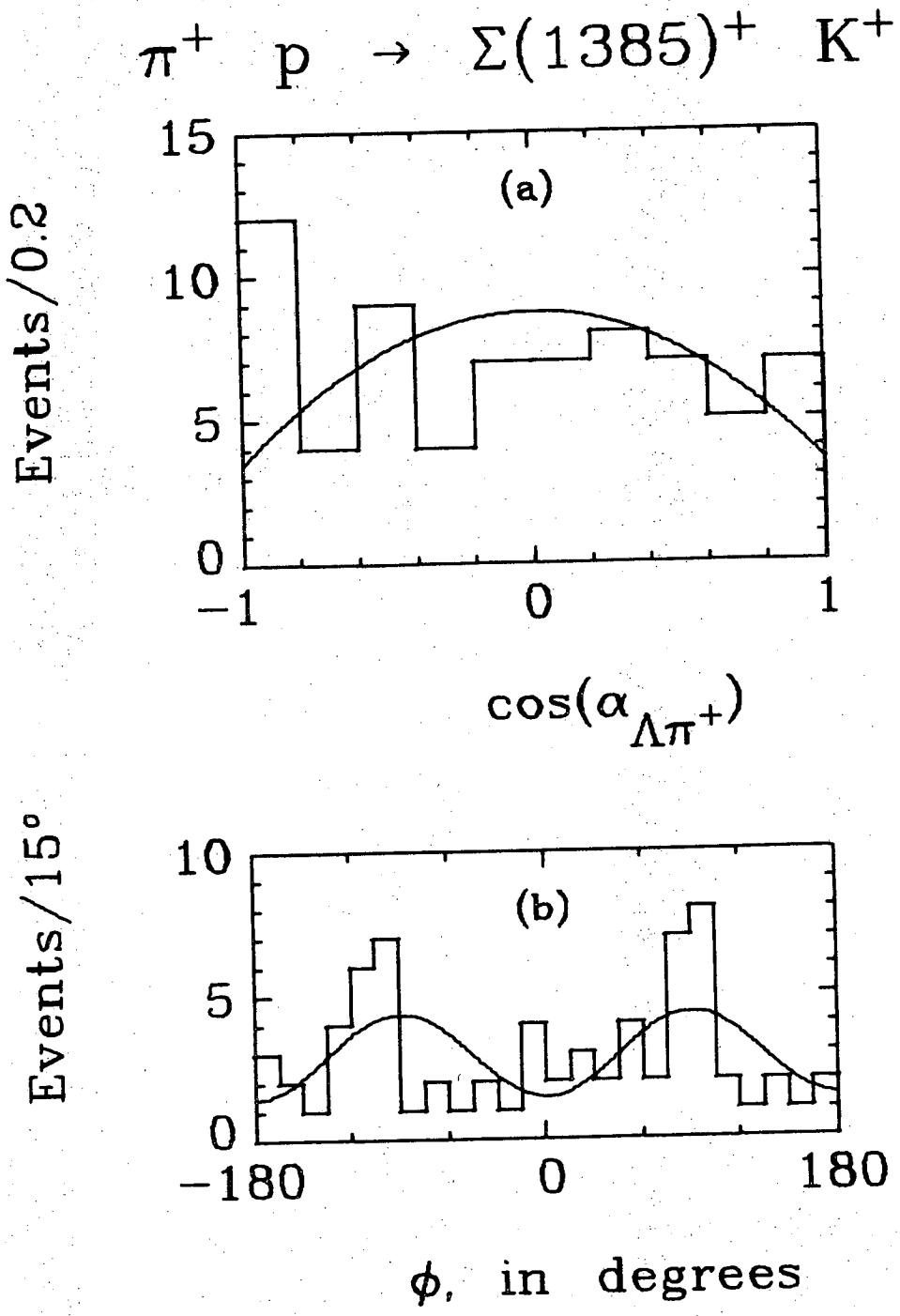

XBL 706-1146

Fig. 24

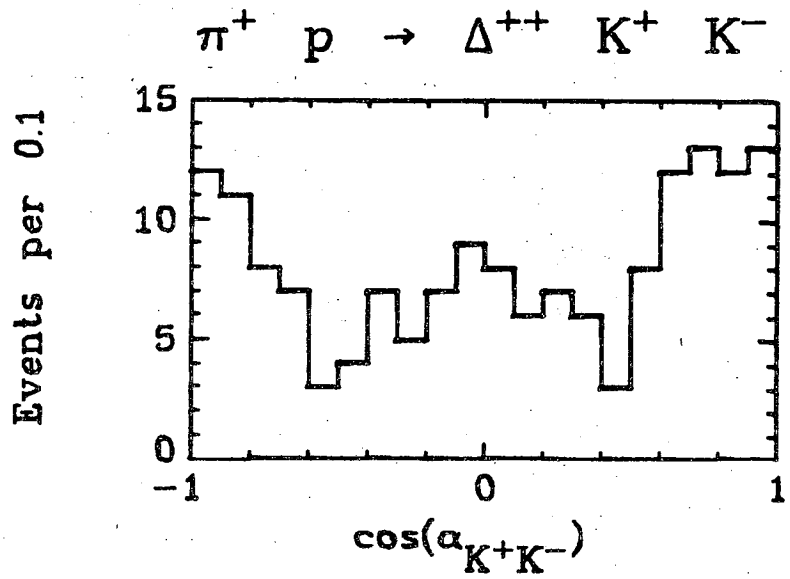

Fig. 25

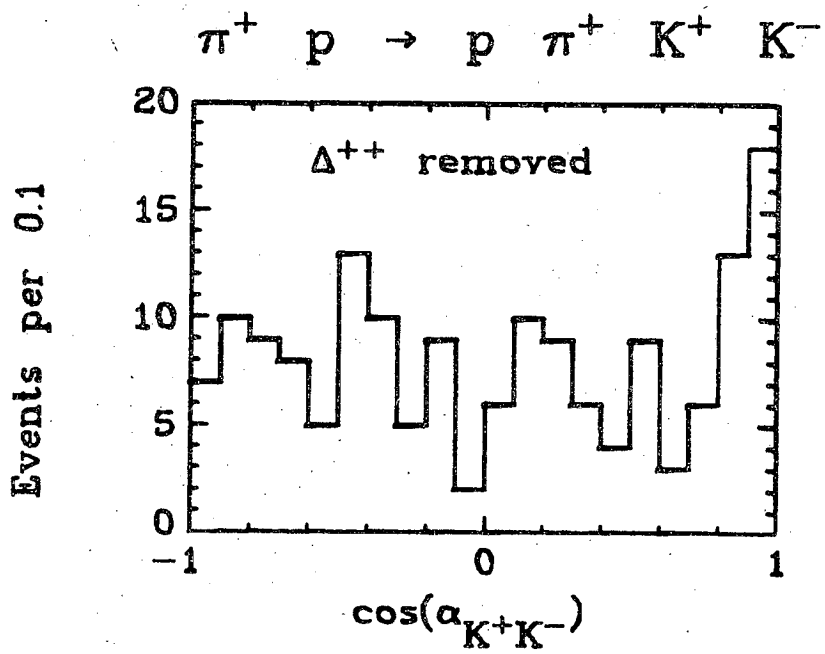

XBL 706-1125

Fig. 26

LEGAL NOTICE

This report was prepared as an account of Government sponsored work. Neither the United States, nor the Commission, nor any person acting on behalf of the Commission:

A. Makes any warranty or representation, expressed or implied, with respect to the accuracy, completeness, or usefulness of the information contained in this report, or that the use of any information, apparatus, method, or process disclosed in this report may not infringe privately owned rights; or

B. Assumes any liabilities with respect to the use of, or for damages resulting from the use of any information, apparatus, method, or process disclosed in this report.

As used in the above, "person acting on behalf of the Commission" includes any employee or contractor of the Commission, or employee of such contractor, to the extent that such employee or contractor of the Commission, or employee of such contractor prepares, disseminates, or provides access to, any information pursuant to his employment or contract with the Commission, or his employment with such contractor.

TECHNICAL INFORMATION DIVISION
LAWRENCE RADIATION LABORATORY
UNIVERSITY OF CALIFORNIA
BERKELEY, CALIFORNIA 94720